Epoxy/Glass Syntactic Foams for Structural and Functional Applications – A Review

Anirudh S[a], Jayalakshmi C. G[b], Anoop Anand[b], Balasubramanian K[a, *] Sikiru O. Ismail[c]

[a] Department of Metallurgical and Materials Engineering, Defence Institute of Advanced Technology (DU), Ministry of Defence, Girinagar, Pune 411025, India.

[b] Composites Research Centre, Research and Development Establishment (Engineers), DRDO, Ministry of Defence, Pune 411015, India.

[c] Department of Engineering, School of Physics, Engineering and Computer Science, University of Hertfordshire, Hatfield, AL10 9AB, England, United Kingdom.

* Corresponding author: K. Balasubramanian, E-mail: meetkbs@gmail.com

Graphical Abstract
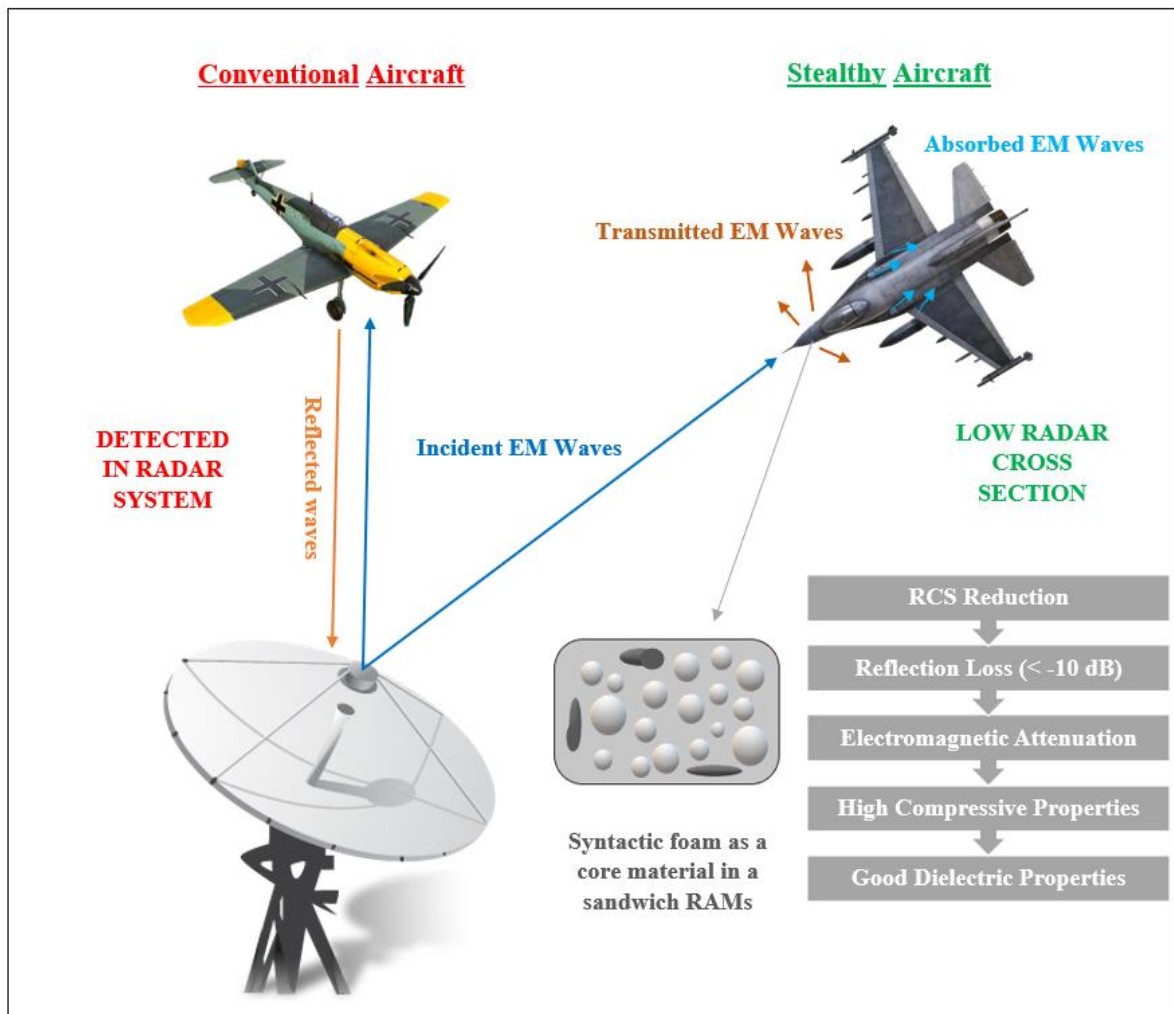
ABSTRACT: Composite materials have improved the fields of aerospace and defense by supporting manufacturing of several structures with high strength-to-weight ratio and stiffness-to-weight ratio, low density, flexible design, low installation cost, outstanding environmental and chemical resistance. More studies are required to reveal what has been done, the present challenges or gaps and future prospects. Therefore, the objective of this article was to present the description, properties, material characterization and applications of the new class of lightweight materials, especially syntactic cellular foam made from epoxy matrix and hollow glass microspheres (HGMs). Their characterizations include density, void measurements, compressive, tensile and modulus properties, glass transition temperature (T_g), wear behaviors as well as their fracture mechanisms during compression, fracture and impact toughness and dielectric properties have been thoroughly reviewed and clearly reported. The effects of varying micro-balloon wall thickness on syntactic foams (SFs) and various methods to improve their mechanical and structural properties have also been elucidated. The unique attributes of these materials offered a wide scope of applications towards developing functional composites. SFs are used in radio detection and ranging (RADAR) system. Based on their dielectric properties, including low dielectric constant and very low loss tangent electrical properties, the effective use of syntactic cellular foam in RADAR absorbing structures (RASs) have been meticulously studied. In this compendious review, the working principles of RADAR, RADAR cross section (RCS) and the factors that affect RCS, reflectivity loss, RADAR absorption materials (RAMs) and their classification were discussed. The enhancement of absorbing performance of glass/epoxy composites, using magnetic fillers, carbon fillers and thin layer nickel (Ni) coating over the dielectric glass fiber and the use of SFs as a core material in a sandwich layer of RAMs to study their electromagnetic (EM) wave absorbing properties have been well addressed. The microwave material interaction for reflectivity loss and various property enhancement methods of RASs were adequately included in this study. Importantly,

this succinct review stands to benefit both designers and developers/manufacturers (researchers, scientists and engineers) of aforementioned multi-functional materials for aerospace and military/defense applications.

Keywords: Epoxy/glass microsphere syntactic foams, Electromagnetic attenuation, RADAR absorbing structures, RCS reduction.

1. INTRODUCTION

Syntactic foams (SFs) are composite materials synthesized in a mechanical way by embedding porous or hollow spheres called micro-balloons (the fillers) in a metal, ceramic or polymer matrix (binder) adhered by a bonding agent. The term 'syntactic foam' was initially formulated by a Bakelite company (1955), produced by embedding hollow phenolic micro-balloons into an epoxy, phenolic binders or polyester matrix to form a lightweight composite. The porosity enclosed in hollow microspheres located inside the thin shell provides a closed-pore foam structure to the material.[1] The presence of microspheres leads to low density, therefore, low weight, lower coefficient of thermal expansion, propensity for highly localized deformation, higher specific strength, and in certain cases, sound navigation and ranging (SONAR) and radio detection and ranging (RADAR) transparency in the composite. Figure 1 shows the scanning electron microscopy (SEM) image of microstructure of syntactic cellular foam. The cell structure is formed with an isotropic nature, that is the same magnitude of physical properties, independent of orientation and the irregularity of its microstructure, unlike polyvinyl chloride, polyurethane and geopolymer foams.[2,3] The properties of SFs are tailorable such that they are effectively used for various applications with enhanced performance when compared with conventional materials.
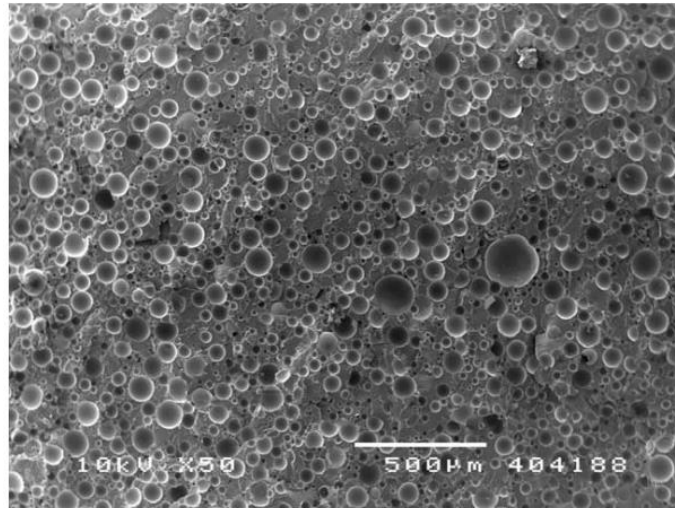
Figure 1. SEM images of SFs.[4]

(Reprinted with permission. Copyright 2005, Elsevier publications).

A substantial enhancement in properties of SFs is accomplished by altering the volume concentration of fillers and a consistent interfacial adhesion between the hollow glass micro-balloons (HGM) and the binder material.[5] For instance, the density is reciprocally related to the volume percentage of microspheres. An increase in volume content reduces the density of the foam. The SFs possess excellent mechanical behaviors with impressive compressive properties.[6] The hollow glass microspheres (HGMs) used in SFs possess several flaws and porosity within the sheath.[7] Additionally, the differing wall thickness of the glass microsphere affects the overall mechanical performance. Therefore, perfectly shaped spherical microspheres are preferred for effective functions.[8]

During the mechanical mixing of the HGM foams with a polymer binder (epoxy), voids are induced. Even, a negligible increase in void content causes detrimental effects on both tensile and dynamic properties. The SEM image of microstructure of syntactic cellular foam with matrix porosity is previously shown in Figure 1. The polymer matrix is most preferred for the syntactic foam (SF) with HGM and a binding agent. Even though, ceramic and metal matrix are high strength materials and withstand high temperatures, but they are susceptible to harsh

4

environmental conditions.[9,10] The unique properties of the HGM reinforced SF are utilised in various fields, including structural, marine and aerospace applications as well as electronics industry and transportation facilities.

2. EVOLUTION OF SF

The syntactic cellular foam is characterized with an excellent tailorable property utilised in various fields to enhance performance. The high-density materials are replaced with low density materials for aerospace applications. For instance, aluminum and related alloys replace iron and steel for structural applications, and now lower density synthetic materials and composites replace them for their strength and impact resistance properties. In this context, SFs are observed to perform exceptionally well in aerospace applications, where low-density materials are desired.

The composite materials used, their limitations and the emergence of SF materials are discussed in this section. Reticulated honeycomb and blown foam materials are used in aerospace applications, as first-and second-generation materials.[11] First generation reticulated honey-comb structures are manufactured in the form of sheets with polymeric materials, which possess low density and numerous voids that separate the wall of interconnection in the material. The reticulated honeycomb is more consistent with a greater strength throughout the whole panel. Its resistance to deformation affects the effective performance of reticulated honeycomb. This makes it unsuitable for complex shaping and bending that is very much necessary for aerospace components, such as exhaust ducts.

Furthermore, in order to overcome the limitations of reticulated honeycomb materials and to improve the performance, expanded foam core materials made of synthetic thermoplastics, such as polyurethane or expanded polystyrene foams are introduced. These are considered to be the second-generation materials, that use blowing agent, such as pentane (a volatile

substance) in the open voids of blown foam. This is done in order to achieve an open-macro cellular structure, which results in expansion of the material on application of heat. The main purpose of the core in the centre of the panel is to create the panel stiffness, while maintaining little weight and resisting the forces created, when the structure is loaded.

The drawback to these second-generation materials is their tendency to expand or contract when exposed to distinct environmental conditions that result in delamination or disintegration of surfaces. The material, when it is wet, causes an elevation in density, because of its sponge-like behavior.[11] Therefore, SF is a third-generation material and is believed to exhibit excellent characteristics, when compared with the previously discussed foam materials. SF differs from expanded foam, where blown foam is expanded with a volatile blowing agent, such as pentane. But, a SF consists of resin in which small diameter, rigid microspheres are embedded.

3. SYNTACTIC CELLULAR FOAM: DESCRIPTION

The syntactic cellular foam is composed of a matrix material and hollow microspheres with a hardening agent. Various materials used, such as matrix, reinforcements and hardener/diluents in SFs and their specifications are discussed in the subsequent sub-sections.

3.1. Microspheres. The hollow microspheres of glass, carbon, polystyrene or phenolic resin have a density varying between 0.15 to 0.46 g/cm³ with a filler size ranging between 10 to 60 μm.[12] These HGM fillers attribute to the compressive properties of their composites. The compressive strength is proportional to density of the composite.

3.2. Matrix

Table 1. Materials Used for Matrix in a Composite Material

Polymer matrix	Metal matrix	Ceramic matrix
Thermosetting:	– Aluminum	– Carbon
– Epoxy	– Titanium	– Zirconia
– Phenolic	– Iron	– Silicon carbide
– Cyanate esters	– Magnesium	– Silicon nitride
– Polyamides	– Zinc	
– Polyurethane	– Copper	
– Unsaturated polyester	– Continuous fiber	
Thermoplastic:	– Graphite	
– Polyethylene	– Super alloys	
– Polypropylene		
– Polystyrene		
– Nylon		

The matrix material in the SF can be made of metal, ceramic or polymer materials with respect to its function, as presented in Table 1.[5] The matrix material chosen contributes to the tensile property of the composite. A chemical surface treatment called silanization is carried out to improve the tensile strength and allows the matrix to form a strong interfacial adhesion between the reinforcements. The addition of fiber materials also improves the tensile strength.

3.3. Hardeners/Diluents. During synthesis, when the matrix is heated up to a certain temperature, its viscosity is reduced[13]. To maintain the viscosity, hardening agents are used to achieve evenly dispersed microspheres during mechanical mixing of the materials. The most commonly used hardeners are amine-based or methyl ethyl ketone-based compounds. The various adjuvants used in SFs and their purposes are presented in Table 2.

Table 2. Various Adjuvants Used in Syntactic Cellular Foam

Adjuvants	Purpose
Chopped fiberglass	Inhibit propagation of cracks.
Nadic methyl anhydride (NMA)	Withstand higher temperatures without degradation.
Rubber tougheners	Increase the toughness of the material and make it less brittle and more impact resistant.
Brominated compounds (BC-58)	Resist ignition of the SF-core material.

4. SYNTACTIC CELLULAR FOAMS: PROPERTIES

The unique properties of the syntactic cellular foams are represented pictorially in Figure 2. The borosilicate glass hollow particles dispersed in the epoxy binder to enhance their capability to resist corrosion and withstand harsh environments.[14] From epoxy resin and hollow microspheres-based SFs, it is observed that longitudinal failure is dominant for the lower density of the foam. While, a layered failure prevails for the higher density.[15] From the epoxy resin-based SFs with hollow microspheres produced by the random sequential adsorption method, it is observed that the cell structure and distribution are improved. The compressive and tensile strengths are observed to be inversely proportional.[16]
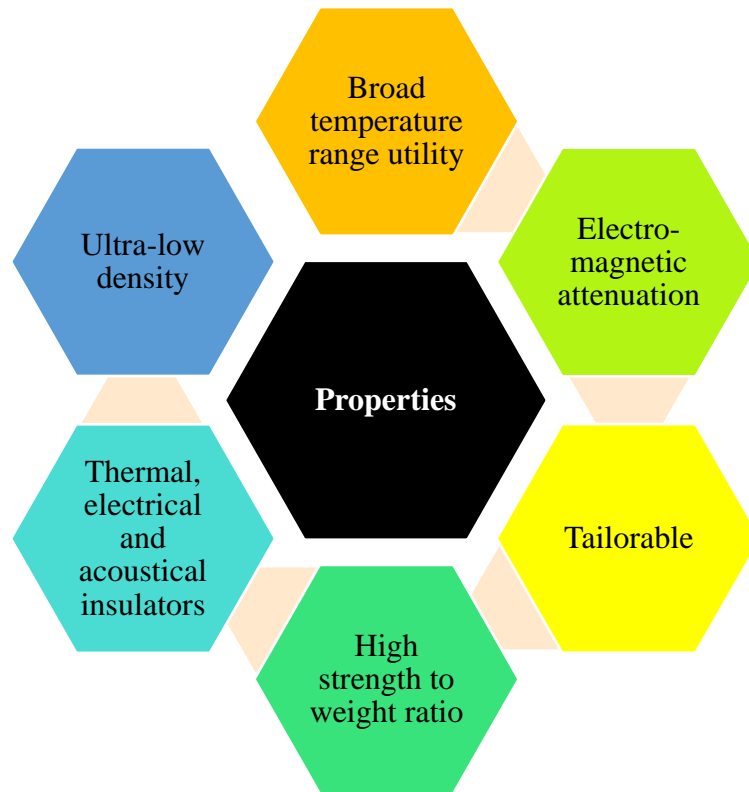
Figure 2. Properties of a syntactic cellular foam.

5. SYNTHESIS: EPOXY MATRIX SF

5.1. Production Parameters. The production parameters that influence the performance of the SF include volume concentration of fillers (HGM) and the epoxy resin matrix, mixing and curing time, post cure treatment, uniform dispersion of HGM, void spaces (due to entrapped air bubbles) and stoichiometric ratio of the matrix.[5]

5.2. Fabrication. SFs have been manufactured by traditional melt techniques, such as extrusion and/or injection molding. The fabrication of epoxy-based syntactic cellular foam constitutes three major steps. Firstly, blending of filler (HGM) and binder (epoxy matrix). Secondly, completing the mold cavity with the blended mixture. Thirdly, curing and post-curing treatment process.[17] The densities of SFs before and after curing are the same.[2] There are various techniques for the production of epoxy/HGM embedded SF. These methods

include: (i) infiltration dye, (ii) direct mold casting, (iii) direct dispersion, (iv) resin transfer mold, assisted by vacuum and (v) direct mold casting and spray techniques.

5.3. Mixing and Degassing. The desired volume percentage of HGM and the epoxy binder are mechanically mixed in a glass mixer. To achieve an undifferentiated slurry and a homogenous mixture with reduced agglomeration, the mixture was thoroughly stirred for 30 minutes. The viscosity of epoxy resin reduces when heating at 60 $^{\circ}$C for 1 hour. This affects the uniform distribution of fillers made of HGM particles in the epoxy resin binder. Additionally, voids or porosity are induced due to the entrapped air bubbles during mechanical mixing.[17] A ratio of 10:3 of epoxy matrix to amine based hardening agents and diluents are used to improve the wettability of the matrix, evenly disperse the HGM fillers and reduce the void contents.

5.4. Curing and Post-Curing Treatments. The blended mixture can be cast in a silicon mold with silicon grease to coat the molding surface for easy ejection of the foam layer after curing. The composite is generally processed at room temperature of 27 $^{\circ}$C for 24 hours, followed by post-curing at 80 $\pm$ 5 $^{\circ}$C for 5 hours.[18] The other method of fabrication is by compression molding. After dispersion, the SF is compression molded in an aluminium or stainless-steel mold for 36 hours and post-cure treatment at 100 $^{\circ}$C for 4 hours.[13,19] The similar method of preparing epoxy/cenosphere SFs was followed by Kiran et al.[20] to determine the tensile behavior of the composite. Singh et al.[21] prepared the epoxy/HGM filler-based SFs, using stir casting method. The effects of reinforcing silica fume on SF were observed. Dubey et al.[22] developed thermoplastic/epoxy-SF for structural applications. The fabrication of SFs with stir casting method is shown in Figure 3.
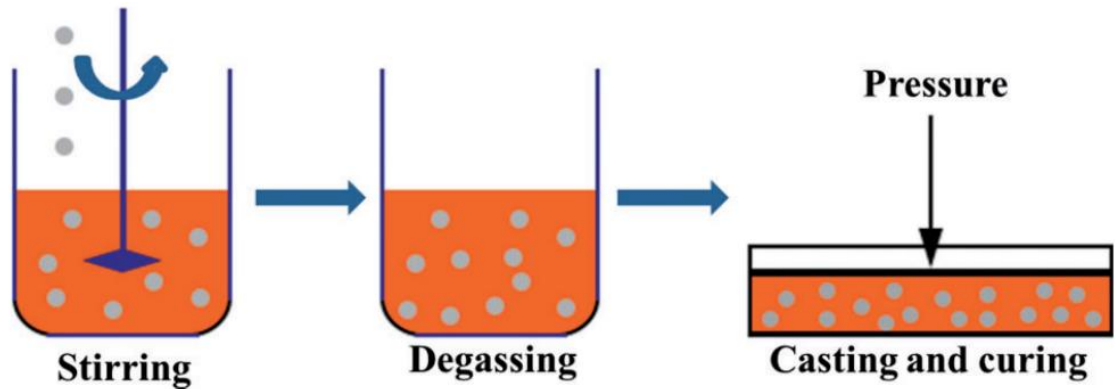
Figure 3. Stir-casting method (SCM) to fabricate SF.[23]
(Reprinted with permission. Copyright 2021, Sage publications).

The epoxy/HGM embedded SFs were fabricated in a few stated steps by Yung et al.[24]: (i) a KH560 coupling agent was applied on the surface of the HGM powder to pre-treat the particles, (ii) Epon 8008 solution, Epon 1031 solution, DICY, 2-MI and HGM were weighed at certain proportions and stirred at a high-speed for 1 hour. Then, (iii) the uniformly formed blend was cast in a mold and the air bubbles and solvent by pumping for 1.0 - 1.5 hours, as the temperature increased from 80 to 145 $^{\circ}$C and (iv) finally, they were heated to 175 $^{\circ}$C for 4 hours for the polymerization to complete. A review on fabrication of SFs by stereolithography of epoxy and acrylate based on HGM fillers was reported by Roques-Carmes et al.[25] On the fabricated three-dimensional (3D) SF, physicochemical analysis has been performed to determine number of microspheres. Criteria for the choice of a polymeric binder were discussed. 3D printing of HGM was prepared by Dileep et al.[26] with high-density polyethylene (HDPE) as a polymer matrix and the suitable printing parameters were enlisted. Jonathan et al.[27] studied carbon fiber (CF) and graphene reinforced composites with high thermal and electrical conductivities, development of new hollow glass particle-filled SF filaments for printing lightweight structures and integration of sensors or actuators during additive manufacturing (AM) of metallic parts. Some of the studies are focused on process optimization or modification to increase the manufacturing speed or tuning manufacturing techniques to enable AM of new materials.

Moving forward, co-continuous HGMs/epoxy matrix SFs were fabricated according to the Chinese patent #ZL 201510594429 by Ding et al.[23] The process of fabrication consists of the following procedures: (1) the HGMs were poured into a quartz tube where one end was blocked by a quartz plate. To make the SFs a close-packed structure, vertical pressure of about 0.5 MPa was applied to the fillers. The system was then placed at 700 $^{\circ}$C for 1 hour in a muffle furnace. (2) a mass ratio of 100:120:1 of epoxy resin, methyl-tetra-hydro-phthalic anhydride and accelerant were blended together. The mixture was stirred and degassed for 30 and 10 minutes, respectively. Then, (3) the blend was put into the filtration equipment and the preformed fillers were placed in a chamber made of PTFE.[28] To keep the system tight, a sealing grease was applied on rubber sealing rings and chamber itself. (4) Vacuum was maintained in the chamber for 10 minutes prior to the injection of the binder and the vacuum pump and compressed air were turned on till the impregnation. When the resin was overflown from the outlet mold, the pump was turned off and the chamber was clamped at the same time. Compressed air was passed continuously into the system until end of flow of epoxy resin. (5) The material was cured at 125 $^{\circ}$C for 2 hours, 150 $^{\circ}$C for 2 hours and 175 $^{\circ}$C for 2 hours. The fabrication of SFs using co-continuous process is depicted in Figure 4.
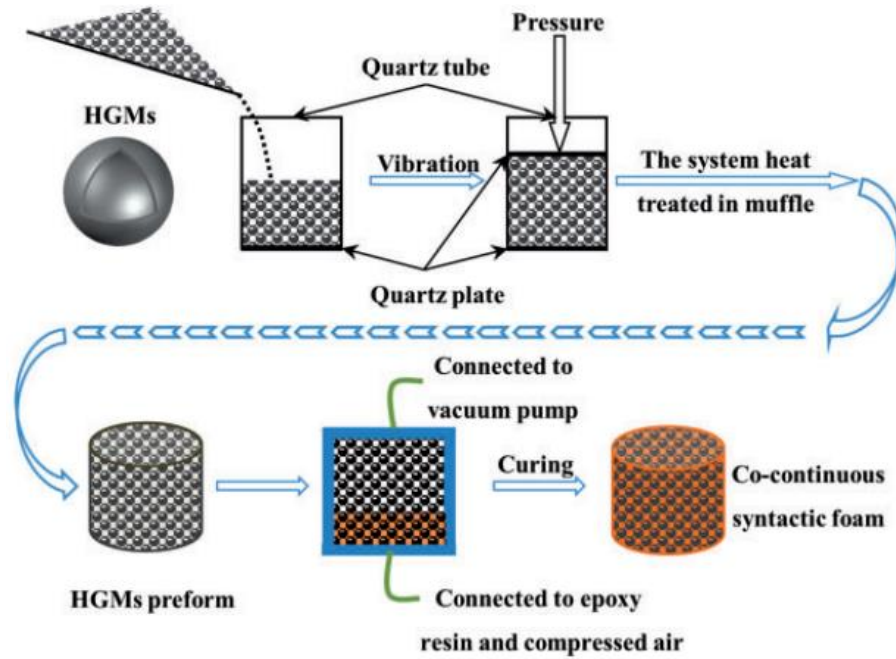
Figure 4. Co-continuous SF fabrication process.[23]
(Reprinted with permission. Copyright 2021, Sage publications).

The influence of ultrasonication on the properties of multi-walled carbon nanotubes/ HGM fillers/epoxy SFs were investigated by Bin et al.[29] with epoxy resin and hardener 2-ethyl-4-methylimidazole as matrix system. The HGM fillers were used and the multi-walled carbon nanotubes (MWCNTs) with diameters of 8-13 nm and lengths of 3-5 μm were mixed to enhance the compressive behaviors of SFs. MWCNTs were well dispersed using ultrasonication method for 10 minutes (500 W, 20 kHz) after mixing with ethanol. A pulsed ultrasound mode operated on for 30 seconds and off for 10 seconds was carried out to avoid structural defects. The excess ethanol was eliminated by placing the blends in a vacuum oven at 80 °C for 24 hours. After that, the HGMs were added with varying volume percentages between 40 - 70% slowly to avoid structural damage to the fillers. Finally, the hardener is added and the mixtures were casted for testing. Ultrasonication process tended to improve the viscosity of the compound, and density was decreased, due to huge porosity generated during fabrication. Post examination of the fractured surface determined the better dispersion of

13

MWCNTs. Better distribution and hydrophobic properties of MWCNTs tended to decrease the water absorption content.[30]

6. HGM FILLER-EPOXY BINDER BASED SF: MATERIAL CHARACTERIZATION

The characterization of HGM filler–epoxy matrix based syntactic cellular foam for density and void measurements, T_g, compressive, tensile and modulus properties, wear behavior, the fracture mechanism during compression, fracture and impact toughness are subsequently elucidated.

6.1. Scanning and transmission electron microscopies. The fracture surface and the structural arrangement of the SF composites are analyzed, using scanning electron microscope (SEM). The fractured tensile and flexural specimens are investigated with aid of SEM. The SFs are non-conductive in nature and the flow of electrons is desired for the fracture surfaces to be viewed clearly, therefore the specimens are gold-coated before being scanned, using SEM.[18] A transmission electron microscope (TEM) of higher magnification can be employed. The dispersion of HGM is investigated, using TEM.

6.2. Density and Void Measurements. The void content in the HGM filled epoxy-based SFs plays a crucial role in their tensile and dynamic properties. A small percentage of 2.5% increase in porosity resulted to detrimental effects on tensile and dynamic characteristics by 20%.[18] The reason was that the HGM filler was a porous material. Therefore, an intermediate degassing step was introduced to eradicate the voids and to maintain them for less than 5%. The theoretical density (ρ_t) of the foam was quantified based on the rule of mixture and the measured density (ρ_m) was determined by ASTM C271-94, with a specimen of $25.0 \times 25.0 \times 12.5$ mm³ dimensions.

Three specimens were formed and mean values were taken. The void fraction, known as Matrix porosity (δ), was determined by Equation 1.

$$\delta = \{100 \ (\rho_t - \rho_m)/ \ \rho_t\} \qquad\qquad\qquad (1)$$

There was a proper interaction between the elements. The perfectly spherical shaped glass microspheres increased the performance of the foam, due to good interfacial bonding. A decline in the theoretical and measured density values with increasing volume fraction of HGM fillers was observed. The measured density is always lower than the theoretical density measures for all volume fractions of HGM fillers.[31] More HGM porosities, along with the presence of void content, decreased the strength and modulus properties of the composite. There was an increase in moisture absorption, which led to diffusion in the sample specimen and piled up in the voids of binders. This was due to the higher void constituent, when compared with theoretical and measured densities. SEM image of the microstructure of SF with HGM fillers and epoxy matrix with matrix porosity is shown in Figure 5.
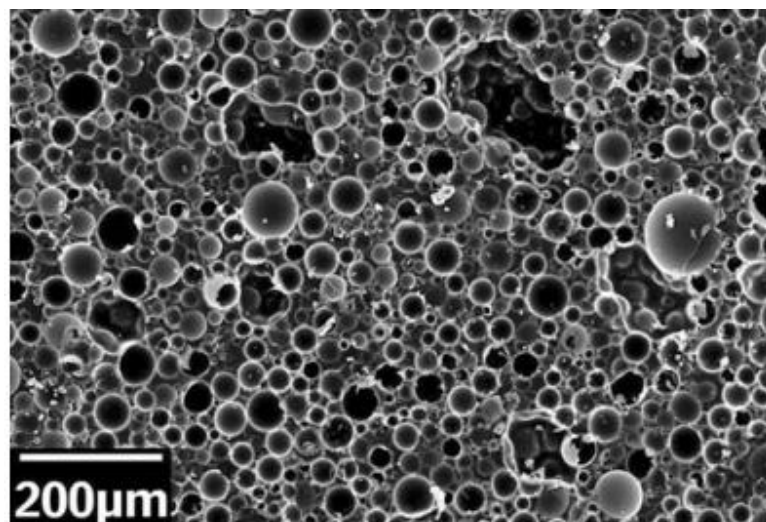

Figure 5. SEM image of microstructure of a SF with hollow microspheres, matrix resin and matrix porosity.[1]

(Reprinted with permission. Copyright 2007, Springer).

6.3 Tensile Properties. The ASTM D 3039 standard has been adopted for the tensile test of SFs. A 100 kN load cell and a 2 mm/min test speed were used. The dimensions of the tensile sample were $250 \times 25 \times 3$ mm. Six different samples were prepared with varying HGM fillers from 10 to 25%.[18] It was observed that with the inclusion of HGM fillers, tensile strength and tensile modulus were improved. This was attributed to the improved interfacial-bonding of fillers with the matrix.[32,33] The highest strength (tensile) was obtained at 20% volume of HGM fillers, which was approximately 65% more when compared with neat resin, due to better interfacial interaction between fillers and the matrix. The highest tensile modulus was obtained at 15% volume fraction of HGM fillers. The tensile strength and modulus of the 25% HGM fillers-epoxy matrix composite reduced. This can be attributed to improved matrix porosity formed by agglomeration and lower resin material, resulting to a reduced interaction between the matrix and reinforcements.[18] Therefore, it is evident that tensile strength and modulus of SFs decrease with addition of HGM fillers, due to increased agglomeration and a weak interfacial adhesion between reinforcement and binders.

SEM is used to determine the fracture mechanism during tensile loading in SF for various volume fractions of HGM fillers, including neat epoxy resin. Brittle failure is observed in neat epoxy matrix composites, as the rupture propagates freely near the surface. The crack surfaces become clearer with the inclusion of HGM. There are three different regions during tensile loading: (1) deboned micro-balloons, (2) fractured micro-balloons and (3) fractured layers, as shown in Figure 6.[18] Increasing HGM volume increases the deboned and fractured microspheres, as a result of enhanced interface bonding between the matrix and fillers. A minimum roughness on the fractured part that constitutes minimum porosity and vice versa was observed, which responsible for the lower strain of the composite when compared with neat resin.
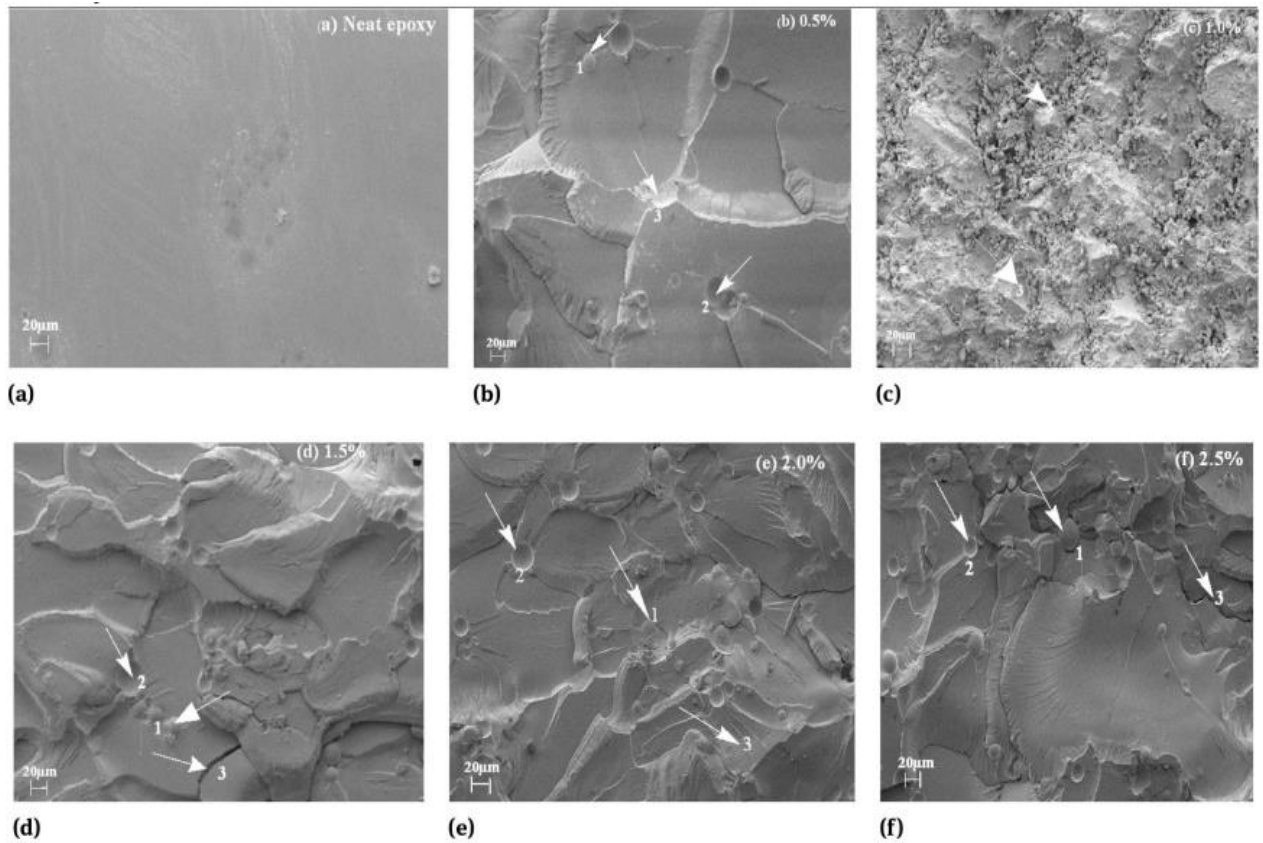
Figure 6. Microstructure of composite material during tensile loading of: (a) neat resin and (b) – (f) increasing HGM filler content, where arrowed areas 1 show de-bonded microspheres, 2 depict fractured microspheres and 3 show fractured surfaces.[18]

(Reprinted with permission. Copyright 2021, De Gruyter).

To study the tensile property with respect to the variation in density across the height or thickness of the slab, Kishore et al.[34] considered the gravity settling effect of HGM filler and epoxy binders during curing to prepare a functionally gradient SF slab with a thickness of 25 mm. Also, sections were 3 mm thick and severed from different cross sections of the SF slab to study the dispersion differences, tensile behaviors and the fracture features of the tensile tested sections. As the percentage of HGM filler decreased, the Youngs modulus of the SFs increased linearly and the tensile strength increase was much higher. Less area between the microspheres with fewer indications related to the binder deformation and pull-out of the HGM

fillers were the features that were observed in the fractography of the specimens with lower strengths. On the other hand, the fractographic features of specimens with higher strength showed more spaces between microspheres, and curvilinear indications of deformation in the binders at binder rich sections.

Gupta et al.[35] conducted research to study the influence of HGM fillers on the tensile characteristics of SF. The test was carried out with sixteen different samples with the density of HGM fillers varying between 0.22 and 0.46 g/cc, as added to epoxy binders. The volume of HGM fillers varied between 30 and 60% in the SFs. The difference in density of the specimen was achieved by selecting the same size, but different wall thickness of the hollow glass fillers. It was possible to directly relate the microsphere characteristics to the tensile behaviors of the SFs through the criteria achieved in selecting the HGM fillers. In this study, the tensile behavior was selectively analyzed with respect to the density and volume content of the glass fillers. With a decrease in the volume content of the low-density microspheres, the tensile modulus of SF was observed to increase. But, with respect to the volume content of high density HGM particles, there was no significant effect on the tensile modulus of SFs. In general, a decrease in volume content and an increase in the density of the hollow microspheres increased the tensile strengths of the SFs.

To determine the tensile characteristics, Schnettler et al.[36] fabricated HGM filler, incorporating epoxy SF with a wall thickness of 1 µm and a mean diameter of 45 µm of the glass microsphere. During the curing process, the viscosity of the liquid resin increased due to the addition of glass fillers. The uncured epoxy binders were blended with SiO_2 nano fillers to counteract the effect of viscosity before the addition of the hollow micro-balloons. The viscosity measurements were carried out, using rheometers. The measured values before and after mixing up of the SiO_2 nano particles indicated that the viscosity reduction was up to 64% after the addition of nano-fillers. The presence of SiO_2 nano-fillers in the SFs indicated a 10%

enhancement in the mechanical stability that is derived from the greater E-modulus of the SFs filler with nanofillers. Due to the addition of SiO_2 nano-particles, a significant embrittlement was observed in the material with the measured tensile strength and elongation values.

The tensile characteristics and the mechanism of fracturing of HGM/epoxy SF with respect to particle clustering were analyzed by Zhu et al.[37] Particle accumulation was considered to be one of the critical factors that affected the effective mechanical performance of the hollow microsphere filled SFs. The random sequential adsorption (RSA) method was adopted in this research, where a 3D microstructure of SFs with varying degrees of particle clusters was studied. For the quantitative analysis of the clustering of particles, a three-phase finite element model was developed, considering the damage features of the interface between the matrix and reinforcements. This method is significant in determining the effect of agglomeration of particles on the tensile characteristics and the mechanism of failure of the HGM filled SFs. For different degrees of particle clustering, the stress-strain response of the SFs was simulated. It was observed that the elastic behaviors of SFs were influenced by the clustering of particles only at in a negligible range. When there was an increase in clustering of particles, the damage strain, fracture strain and tensile strength of SFs decreased gradually, according to the quantitative analysis of the simulation results. An increase in the degree of clustering from 0 to 0.8 caused the tensile strength to decline by up to 10.7%. It was also observed that the interfacial debonding and the fracture in HGM fillers were the two modes of final fracture in SFs, triggered by particle clustering. The interfacial de-bonding was due to the stress concentration increased by the clustering, causing early damage to the interface region. On further loading, the stress concentrators acted as crack initiators.

In addition, the tensile characteristics of hollow microsphere/epoxy SFs reinforced with carbon nano fibers were investigated by Gupta et al.[38] Four different carbon nanofibers (CNFs) reinforced SF samples with HGM fillers with two varying wall thicknesses in two different

volume fractions were prepared. The results showed that the addition of CNFs enhanced the tensile properties of the SFs. The specific tensile modulus and specific tensile strength of CNF/epoxy composites were less than that of SFs. Higher tensile strength (about 50% increment) was observed in the CNF reinforced SFs, when compared with the plain SFs. The dispersion (homogeneous) of CNFs in the SF was one of the important factors that influences the mechanical properties. As the specifications of the fiber were decreased, the surface area for the same volume content increased. This enhanced the bonding between them, which resulted to improved strength and stiffness of the composites.

Salem et al.[39] researched to enhance the mechanical characteristics of epoxy/glass filled SFs by incorporating carbon nano fibers and halloysite nanotubes. The microstructure of this material was analyzed by X-ray micro-computed tomography. The structural properties and mechanical behaviors of SFs embedded with CNFs and halloysite nanotubes (HNTs) were analyzed and are subsequently reported. A standard process to incorporate nano-materials into the epoxy binder with less or zero agglomeration and the tensile characteristics were determined. The compressive characteristics of SFs improved drastically, but there was a drop in tensile properties, such that the overall tensile properties achieved were as large as 119 and 167% for strength and modulus respectively for 0.5% of CNFs. With the addition of 0.125% of HNTs, the tensile properties increased, but later reduced significantly beyond 0.125%. The tensile properties of SFs were better with 0.125% addition of HNTs, as the density of HNTs provided greater resistance to the propagation of cracks when compared with CNFs.

Belingardi et al.[40] studied the he epoxy SF with a 30% volume content of HGM fillers modified by adding 1% volume percentage of graphene nano-platelets. Graphene nano-platelets and HGM filler were treated with 1-pyrenecarboxaldehyde in xylene and carbon black (CB). The best enhancement in mechanical properties was observed with the SFs with CB. The volume content of 1% of carbon fillers and 30% of HGM fillers in SFs enhanced the elastic

modulus of the material. When compared with neat SFs, the CB reinforced SFs showed better tensile properties; up to 5 and 16% increase in tensile modulus and strength, respectively.

6.4 Effect of Wall Thickness on SFs. A novel approach was carried out by Gupta et al.[13], where the density was varied, while maintaining a constant volume fraction of HGM fillers. In order to achieve this, the HGM fillers selected were almost the same size with varying wall thickness. The mechanical properties, such as compressive behaviors and fracture characteristics of SFs were substantially impacted by the effective thickness of the wall of the fillers. Figure 7 shows the single particle system and the coordinate system. Let r_i and r_o represent the internal and external radii, respectively. The radius ratio (η) is the ratio of the internal radius (r_i) to the external radius (r_o), as represented in Equation 2.

$$\eta = r_i / r_o \tag{2}$$

The volume of material with HGM filler is represented in Equation 3.

$$V = (4/3)\,\pi r_o^3\,(1 - \eta^3)\,r_o \tag{3}$$
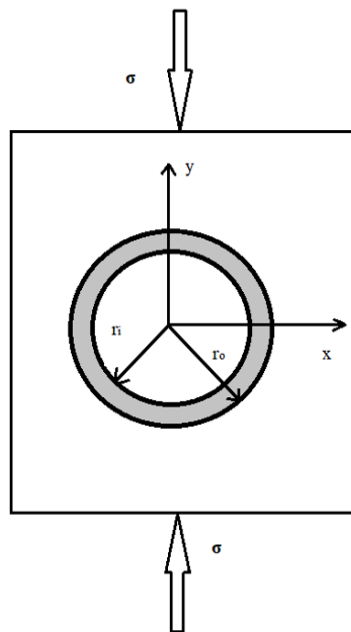
Figure 7. Single particle system and the coordinate system.

The composites filled with solid particles and microspheres exhibit similar deformation behavior when fracture does not occur during the deformation process. In case of micro-balloon matrix composite failure, fracture in the micro-balloon is not the failure mode. The void developed surrounds the fillers generated, due to interfacial break down that is considered to be an ellipse in 2D space, as shown in Figure 8. The maximum stress in the matrix is represented in Equation 4.

$$\sigma_{max} = [\ 1 + 2(a/b)]\ \sigma_{nom} \qquad\qquad (4)$$

Where, a and b are the major and minor axes of an ellipse induced around microspheres.
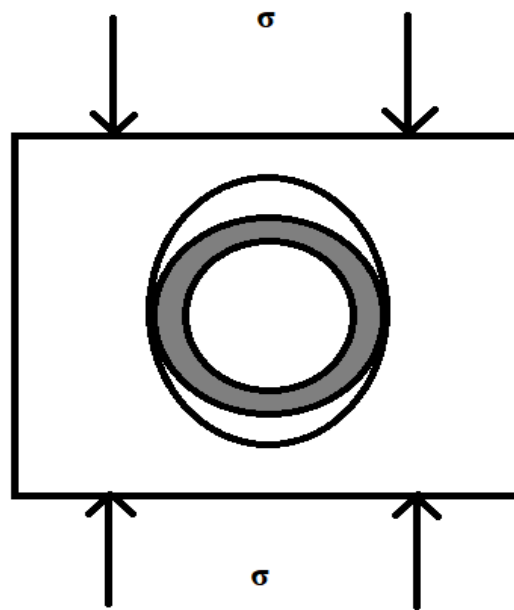
Figure 8. Interfacial failure, as a primary mode of failure in composite.

The stress state of the microsphere in the composite fractures is completely different from that of a solid particle composite material. The failure of a brittle part gives rise to small pieces with a non-uniformness between each other. A mismatch in fragments is produced as: (a) these pieces try to align themselves in the direction of applied tensile load and (b) due to the revolving of these pieces as a result of shear loads or stresses.[13] These fragments possess

22

random shapes and orientation. Therefore, calculation of debris volume is difficult after the fracture of microspheres. On further loading, it is assumed that tiny spherical fragments are generated from the fracture of micro-balloons. It was observed that the critical radius ratio value was equal to 0.71. There was no additional stress generated in the matrix during fracture of microspheres for higher values of radius ratio. All types of micro-balloons investigated possessed a radius ratio greater than 0.71. The effect of wall thickness on drilling of epoxy/HGM filler SFs was studied by Ashrith et al.[41] and it was concluded that the increase in wall thickness of the glass microspheres improved the cutting resistance of SFs and hence the thrust force needed to be increased.

6.5. Compressive Properties. ASTM – D695 – 96 standards have been selected for compression testing of SFs. For comparison, the tests were carried out on both unreinforced and reinforced composites. The specimen specification was 12.7×12.7 mm^2 and the height was 25.4 mm. The rate of cross section head was retained at 1.3 mm/min for five different test sample materials. The corresponding curves for stress – strain were obtained for all the test specimens. The compressive modulus and peak strength values were determined from the graph. It was prominent from the results that there was an increase in modulus and the peak strength with diminishing microsphere's radius ratio (η). They were improved up to two times, due to a decrease in radius ratio η from 0.922 to 0.863.[13] There was a decrease in stress value at the end of the elastic zone, known as the plateau region, in which damage tolerance was characterized. The fracture mechanism was the crushing of microspheres. The empty space in the microsphere was occupied by debris that led to densification of material during compression. Therefore, it can be concluded that the mechanical characteristics can be enhanced by varying the wall thickness of the HGM, while enduring a constant volume percentage of HGM fillers in the composite.[6,42] The compression loading test procedure of SF has been previously shown in Figure 7.

Moving forward, Sankaran et al.[42] fabricated the SF by mechanical mixing of epoxy resin and HGM to study its compressive behavior. The glass micro-balloon volume fraction was 67.80% with a size ranging between 44 to 175 µm. The average particle size was considered to be 80 µm and the bulk density of the particles was 0.254 g/cc. The density of epoxy resin was 1.1 g/cc and the resin to hardener ratio was maintained at 100:38 by weight. The curing of the SF was done with a ratio of 1.52:1.00 of weight of resin to reinforcement for the SF slabs. After curing, the density of this slab was observed to be 0.433 g/cc with 67.8% micro-balloons, 23.8 % of epoxy resin and 8.4% of void content by volume. This research was conducted with the intent of determining the deformation and fracture features of the foam under compression, stress-strain curves and the effect on compressive strength with respect to aspect ratio (ratio of height/width). Four different specimens with varying aspect ratios were produced for the compressive test. The ASTM D695-91 test standards were considered for the low volume content of micro-balloons, because the materials showed the characteristics of epoxy resin. For compression loading tests, ASTM D1621-94 test standards were employed in this research because, for higher volume fraction of micro-balloons, the material behaved similar to a cellular structure. A curve was plotted against compressive stress *versus* engineering strain. For higher aspect ratio, this curve was divided into three regions: (i) region 1 corresponded to the elastic behavior of the composite; (ii) region 2 (plateau region) corresponded to the energy absorbed by the material during the crushing of reinforcement particles. (iii) At the end of region 2, an increase in stress was observed, which was considered as region 3. But, for lower values of aspect ratio, there was no decline in stress values after maximum value; stress became constantly increasing after region 2 (plateau region). For higher values of aspect ratio, during compression, the mode of failure of SF was due to the shear type of cracks, and for low aspect ratio values, the mode of failure was due to the formation of wedge-shaped cracks.[34] Thus, it

was recommended that the value of the aspect ratio must be kept as low as possible for uniform compression, neglecting the shearing effects.

Woldesenbet et al.[6] conducted tests to determine the parameters that led to tensile, compressive and shear fracture in SFs as the core material in sandwich structures, using microscopic observation after compressive testing. This examination was repeated for SF reinforced with glass fibers in a cladded structure for materials with varying aspect ratios. The variation in local stress conditions and the outcomes of fractured surfaces of both SF core in sandwich material and reinforced SF were observed from the analysis of microstructure in flatwise and edgewise orientation after compression test. In general, the compression mode of failure can be determined by the presence of fragments of microspheres on the fractured surface. If there were no fragments along the surface, it can be either a tensile or shear fracture. The local stress conditions, as experienced by the material were represented by the features of fragments or debris after loading. In order to differentiate between shear type and tensile fracture, it was identified that banded structures (step-like structures) were visible during shear failure, as the crack propagation took place along different planes. In the case of tensile fracture, there was no particular pattern, but the undamaged particles were visible everywhere with very few damaged particles. The failure of reinforced SF with fibers, vertical splitting of the material took place only in one direction.

Furthermore, Kim et al.[15] studied the failure mechanism of SF with varying densities ranging between 0.09 to 0.15 g/cc under compression. A soda-lime-borosilicate glass microsphere with an average density of 0.125 g/cc, measured using an air comparison pycnometer, was embedded in the mixture of epoxy resin and the hardener. The viscosities were also measured for hardener and epoxy resin, using a Brookfield syncro-electric viscometer. During compression, the SF materials failed either by longitudinal splitting or layered crushing. The longitudinal splitting mode of failure was observed in foams with lower

density and the sequence of failure is as follows: (i) a few cracks are formed along the length of the specimen, (ii) the cracks widen by increasing the compressive load and (iii) one end of the sample failed, followed by the lateral expansion of the cracks. The failure sequence of low-density SF was similar to that of the direction of crack propagation in the foam that contained higher volume content of glass in epoxy resin. The failure mode of layered crushing was dominant in relatively high-density SF by breaking the glass micro-balloons and then the occurrence of densification by accumulation of broken fragments during compression. It was assumed that the initiation of failure should be in one of the weakest areas and then the crack should have propagated, causing fracture in the material.

A novel approach has been carried out by Gupta et al.[43], where the density is varied while maintaining a constant volume fraction of HGM fillers. In order to achieve this, the HGM fillers selected were almost the same size with varying wall thickness. The mechanical properties, including compressive behavior and fracture characteristics of SFs were substantially impacted by the effective thickness of the wall of the fillers. Let r_i be the internal radius and r_o be the external radius. The radius ratio (η) is the ratio of the internal radius (r_i) to the external radius (r_o). The ASTM – D695 – 96 standards were selected for compression testing of SFs. For comparison, the tests were carried out on both unreinforced and reinforced composites. The specimen specification for this test was 12.7×12.7 mm^2 and the height was 25.4 mm. The rate of cross section head was retained at 1.3 mm/min for five different test sample materials. The corresponding curves for stress – strain was drawn for all the test specimens. The compressive modulus and peak strength values were obtained from the graph. It was prominent from the results obtained that there was an increase in modulus and the peak strength with diminishing microsphere radius ratio (η). The values improved up to two times, due to a decrease in radius ratio η from 0.922 to 0.863. There was a decrease in the stress value at the end of the elastic zone, known as the plateau region, in which damage tolerance was

characterized. The fracture mechanism was the crushing of microspheres. The empty space in the microsphere was occupied by debris that led to densification of material during compression. Therefore, it can be concluded that the mechanical characteristics can be enhanced by varying the wall thickness of the HGM, while enduring a constant volume percentage of HGM fillers in the composite.

Chen et al.[44] addressed the effects of adiabatic temperature rise and environmental temperature variations on the compressive characteristics of epoxy SFs. The compressive stress-strain curves were plotted and the modes of failure at varying strain rates were determined. The foam density was obtained to be 0.77 g/cc and the T_g was 70 °C. It was observed that, during dynamic compression, the specimen experienced a slight increase in temperature, and therefore the effect was negligible on the specimen during adiabatic temperature rise. On the contrary, the dynamic properties of the SFs were significantly affected by the ambient temperature change. The foam initially hardened with declining temperature. However, there was a strong dominance of thermal softening and damage-softening mechanisms below the transition temperature. This resulted to softening of the foam. The microstructure of SFs at various temperatures is shown in Figure 9.
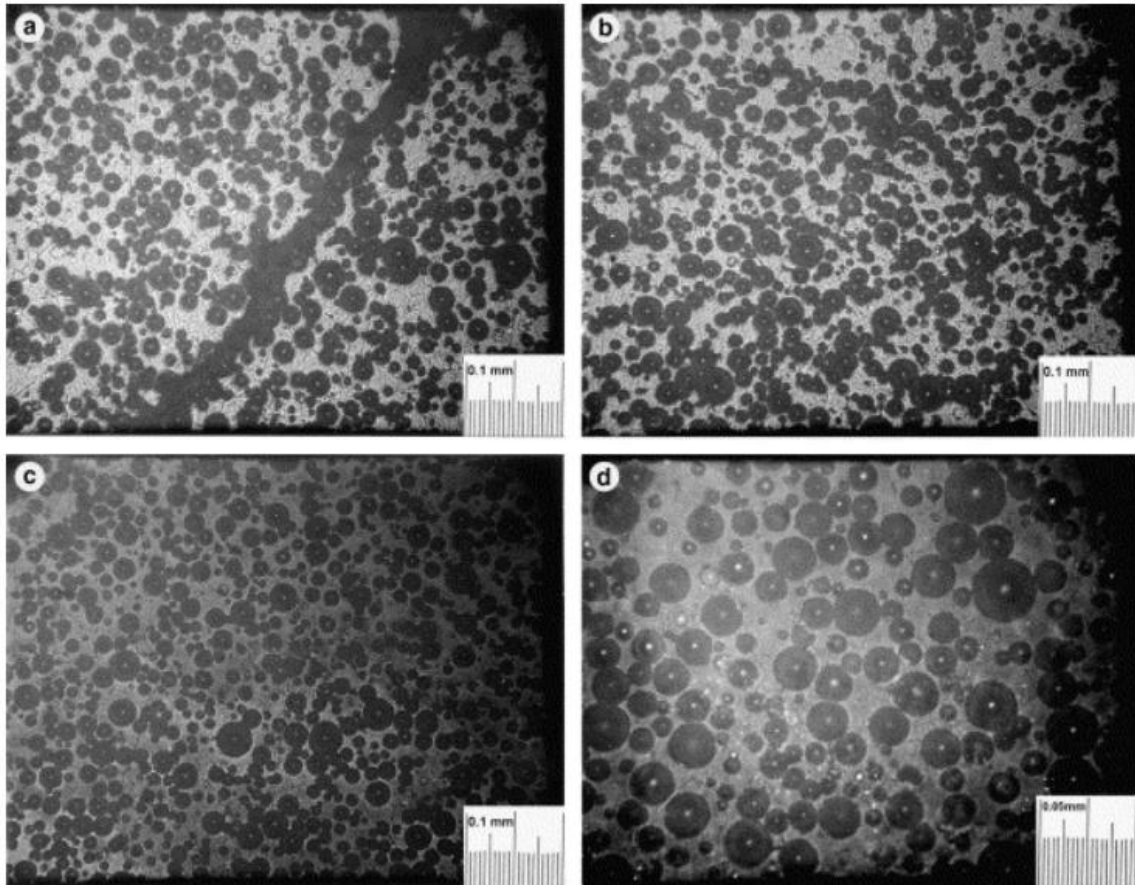
Figure 9. Microstructure of SFs at various temperatures: (a) 0, (b) 23, (c) 74 and (d) 74 °C. [18,44]

(Reprinted with permission. Copyright 2004, Elsevier publications).

Reed et al.[45] reported the effect on dynamic compressive properties, failure modes, and energy dissipation of glass/epoxy SFs with respect to varying strain rates. The strain rates applied to the SF ranged from 0.001 to 4000 s^{-1}. The volume content of the glass micro-balloon was 70% with a size of the particle equivalent to 100 µm, a bulk density of 0.3 g/cc and a crushing strength equivalent to 30 MPa. The strain rate affected the epoxy resin and caused non-uniform deformation and localized damage. The two modes of failure were: (i) crushing of microspheres from the centre portion of the sample and (ii) initiation and propagation of shear cracks from one of the corners. At higher rates, epoxy binders was stronger and the crushing of glass fillers dominated the de-bonding of binder and fillers under dynamic loading

conditions, requiring higher energy absorption in the SF. At higher strain rates, the shear crack developed through the glass fillers instead of crossing them or de-bonding them. The energy absorption capability, localized stresses and fracture resistance increased with log of strain rates. The volumetric strain was proportional to the nominal strain and increased with the rate of strain.

In order to investigate the mechanical properties, Swetha et al.[46] fabricated SFs with different densities, using stir casting method. The quasi-static compressive test was performed at the rate of 0.001 s^{-1} to determine the effect of microsphere fraction and wall thickness of the micro-balloons on the mechanical response of the foam. This experiment was conducted with three different volume percentages of microspheres, ranging between 0 to 60% of the total volume. The increase in volume percentage of the glass fillers decreased the compressive modulus and strength of the foam, but the compressive properties improved with an increase in the wall thickness of the micro-balloons. Axial splitting and shear cracking were the two modes of failure in the SF, which was quite similar to the failure mode of cellular structures, as shown in Figure 10. The stable or unstable nature of the stress-strain curves and the fracture behavior of SFs were dependent on the wall thickness of the glass filler.
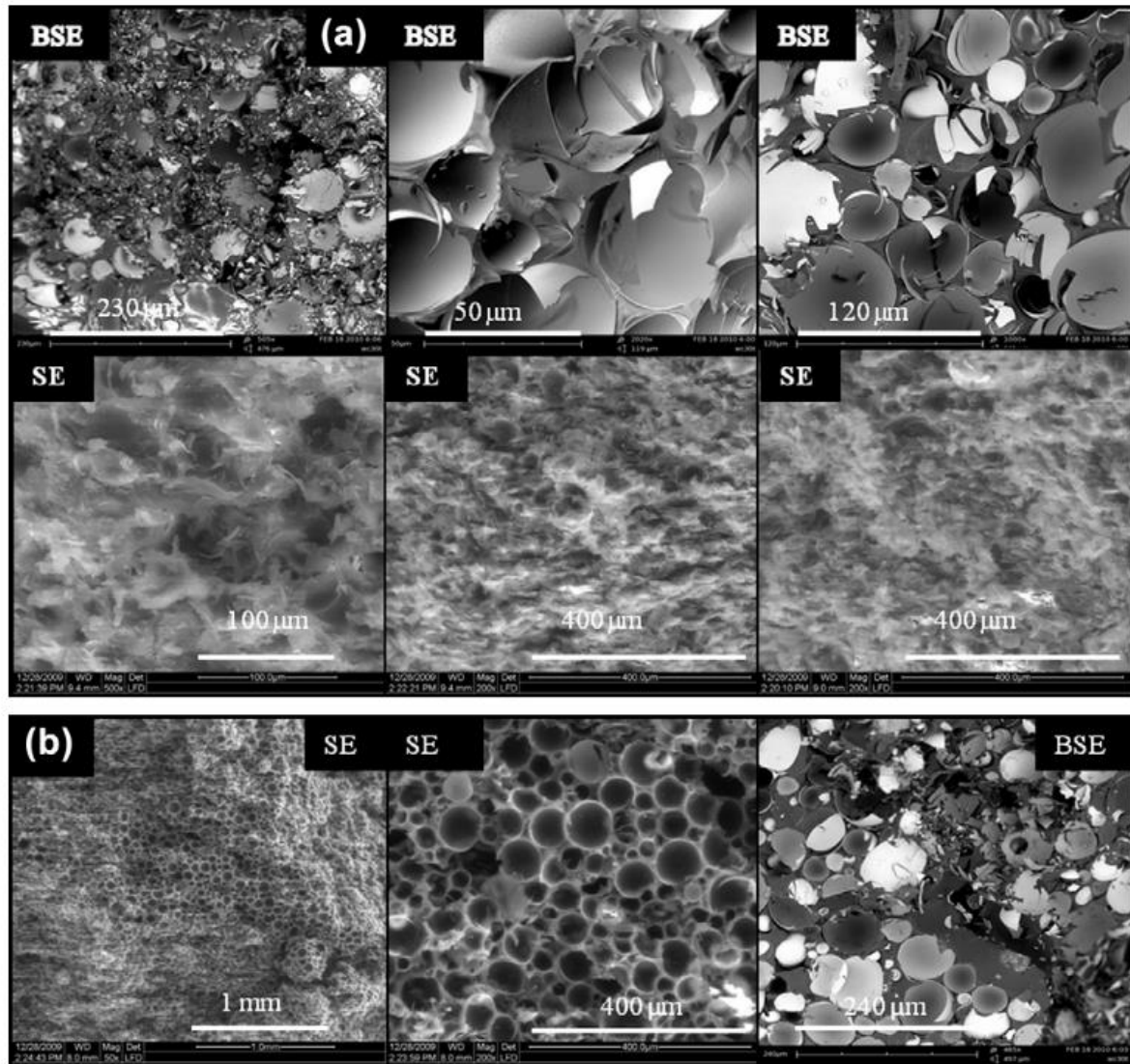
Figure 10. Fractured surfaces of SF100-60 foam, showing (a) crushed microspheres and (b) small amount of debris.[18,46]

(Reprinted with permission. Copyright 2011, Elsevier publications).

In a study carried out by Salem et al.[39] to enhance the mechanical characteristics of epoxy/glass filled SFs by incorporating carbon nano fibers and halloysite nanotubes. The microstructure of this material was analyzed by X-ray micro-computed tomography. The structural properties and mechanical behaviors of SFs embedded with CNFs and carbon nanotubes (CNTs) were analyzed. A standard process to incorporate nano-materials into the epoxy binder with less or zero agglomeration was determined. A large impact on compressive

characteristics was observed in the SF for small quantities of nano fillers. The addition of 0.25% of carbon nano fibers to the SFs increased the compressive strength and modulus by 180% and 250%, respectively. Increase of 164 and 245% in compressive properties was achieved by adding 0.5% of halloysite nanotubes.

Also, the epoxy SF with a 30% volume content of HGM fillers was modified by adding 1% volume percentage of graphene nano-platelets. Graphene nano platelets and HGM filler were treated with 1-pyrenecarboxaldehyde in xylene, and CB by Belingardi et al.[40] It was observed that both SF and the SF with CB possessed almost the same values of compressive strength. Moreover, the SF and the SF with CB content exhibited better peak stress of 550 MPa, when compared with pristine epoxy resin of 250 MPa. The compressive modulus of the SFs with reinforced CB was greater, when compared with that of SF. The samples incorporated with graphene platelets produced poor mechanical properties, especially in strength due to agglomeration and formation of porosity in the binders.

Zhang et al.[47] fabricated a HGM filler/epoxy SF reinforced with hybrid functionalized carbon nanotubes (CNTs) and their mechanical characterization was studied. Three non-covalent modifiers, polyethylene glycol (PEG), chitosan (CS) and polymethylphenyl siloxane (PMPS), were used for carboxylation of CNTs. The fracture morphology of SFs was described, where micro-balloons are removed and dispersed at the fracture surface from the binders during the fracture mechanism. During compressive loads, the CNTs replaced glass fillers and withstood greater loads and made the crack propagation difficult. The compressive strength of SF was enhanced with the addition of MWCNTs to 0.3% of volume. On further increase of the volume content, the strength declined due to an increase in the internal porosity of the foam and a decrease in the bonding energy between the binder and the fillers.[48] Therefore, the hybrid functionalized SF decreased the agglomeration of CNTs without weakening the strength of

covalent bonding in epoxy binders. The CNTs incorporated with polymethylphenyl siloxane (PMPS) possessed the best distribution in the epoxy binders and higher compressive strength.

Kim et al.[15] studied the two modes of failure in SFs, which were: (i) longitudinal splitting and (ii) layered crushing. It is understood that the longitudinal failure was dominant at a lower density of the composite and the layered failure was prominent at a proportionately higher density. The fracture mechanism of SFs, due to compressive loading occured in three steps: Firstly, shear crack initiation due to shearing force or stress and onset of vertical cracks. During stage 1, the cracks developed in the form of wedge-shaped fragments due to shearing (Figure 11a). Secondly, enlargement of vertical cracks (Figure 11b). Thirdly, vertical dissociation and failure of the sample. This grew in vertical direction on further application of load and failed (Figure 11c).[13] It was observed that with the decrease in radius ratio (η), vertical splitting became increasingly eminent. The higher the stiffness value, the more its secondary tensile stresses that led to early formation of vertical cracks.
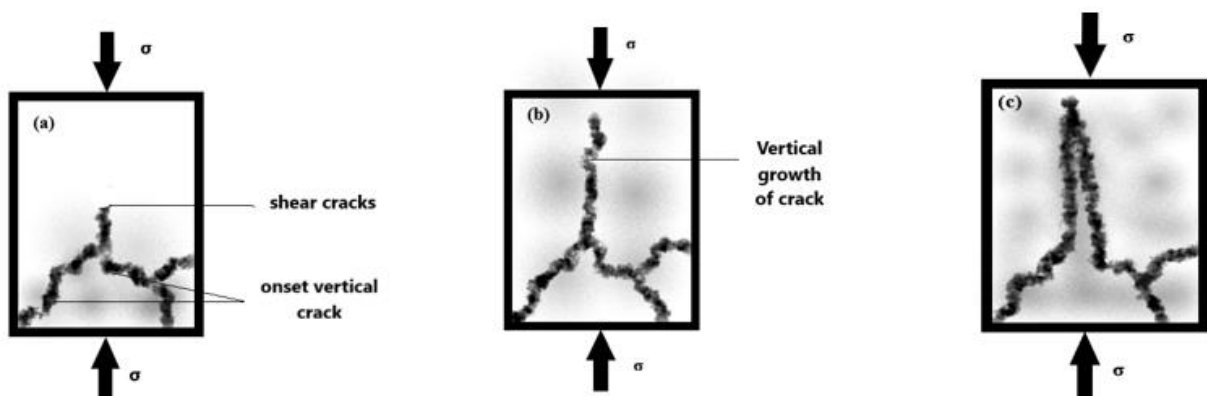
Figure 11. Fracture mechanism during compression, showing (a) formation of crack during shearing, (b) enlargement of vertical crack growth and (c) vertical dissociation of the sample.

6.6. Glass Transition Temperature. Gupta et al.[35] interpreted that the thickness of wall and volume percentage of the HGMs have a greater consequence on T_g. Binder, adjuvants and hardener were mixed in the ratio of 83.5:4.4:12.1 by volume. The T_g of the pure binder resin

was measured to be 117.89 °C and the T_g of all the other SFs was comparatively smaller than that of the neat matrix resin.[1] The interfacial responses between the HGMs and the binders contributed to the declining T_g. The T_g was strongly affected by the volume fraction of HGM fillers, but the wall thickness has less influence on them. The functionally graded SFs (FGSFs) possessed a clear gradient of T_g that was fabricated based on variation in micro-balloon volume fraction. But, the FGSFs that were fabricated based on creating a variation in microsphere thickness of wall never possessed an abrupt gradient in T_g. Solid particles and hollow particle composites exhibited a greater difference in their properties. For instance, in solid particles, a change in volume content of particles was progressed by varying the volume content of glass material that led to a change in interfacial area between particles and resin. Therefore, the results always showed a total effect of volume percentage and interfacial area. In case of hollow particle, by varying wall thickness of the micro-balloon it was possible to vary glass particle content with a constant volume fraction. This approach made effect of glass particles and interaction area independent of each other. The measured T_g values of SFs containing same HGM fillers volume fraction of varying wall thickness established that there was no greater impact on T_g, due to variation in wall thickness. Therefore, it can be concluded that the T_g was attributed to volume contents of various constituents. Hence, it was evident that interfacial reactions consequently affected the T_g of the composite.[49]

SFs with oxazolidone-modified epoxy resin using glass microspheres as reinforcement fillers with varying densities were processed by Robert et al.[50] The impact of various standards of fillers and their concentration on the mechanical, thermal, thermomechanical and flammability characteristics were studied. Dynamic mechanical analysis (DMA) was basically used to determine the maximum-use temperature to identify the thermal transitions temperatures and T_g. It was observed that the epoxy binder modified with oxazolidone was stable (thermally) till around 300 °C. By dispersing the microspheres evenly, T_g of the

composites improved from 90.0 to 115.0 °C. The thermal conductivity of the SFs decreased with decreasing binder: filler weight ratio. The specific heat of the different composites was in the range of 0.32 to 0.44 cal/g/°C, and the coefficient of thermal expansion was 10^{-6} /°C for all the systems.

Moving forward, Woldesenbet et al.[51] developed the first bucky SF, made up of carbon nanotube-ionic liquid hybrid. Mechanical and electrical characteristics of SFs were expected to improve since ionic liquids (ILs) acted as a dispersing and binding agent between carbon nanotubes (CNTs) and the binders. Differential scanning calorimetry (DSC) was used for thermal analysis to ensure the complete curing of samples in the presence of IL. Fourier transform infrared (FTIR) spectroscopy was used to verify the formation of the hybrid for Cation-p interaction of CNTs and the used imidazolium-based IL. The parameters for thermal analysis of the post-cured samples were carried out at 10 °C/min heating rate at temperature range of 50–250 °C. All samples were studied under a nitrogen atmosphere with a constant flow rate of 20 ml/min. Thermal analysis with DSC of the post-cured samples verified that the samples were fully cured in the ILs. Electrical conductivity of bucky SF was enhanced by five times in terms of magnitude, where the traditional insulator SFs were converted to a conductive one.

Epoxy/HGM filler-based SFs that could withstand the use-temperatures ranging between 106 to 175 °C were fabricated with an appropriate amine hardener. In a single cantilever mode, the SFs were characterized for dynamic mechanical properties by Sankaran et al.[34] Over a wide range of temperature, frequency and time, the storage modulus, loss modulus and tan δ values were tabulated. The density value of SFs was nearly 0.45 g/cc made from a cycloaliphatic amine hardener, aromatic amine hardener-I, aromatic amine hardener-II. The formulations of epoxy varied from room temperature to elevated temperature curing systems. The viscoelastic information measured from this analysis was very useful for development of material and

quality control. The T_g values of the SFs were 130.7, 151 and 202.4 °C respectively for different hardeners. Usually, the T_g values for the foams were greater than that of pure resins. The interpreted maximum use-temperatures of the foams were 106, 125 and 175 °C, respectively. Compared with the pure resins, the reduction in the storage modulus of SFs with increasing temperature was less. For the cycloaliphatic amine based-system, the damping factor was observed to be higher.

6.7. Wear Behavior. The influence of HGM on the dry sliding wear mode of epoxy binder SF was investigated in this section. Additionally, wear rate W_t and friction coefficient (μ) were also studied. Three different samples of $12.0 \times 12.0 \times 25.4$ mm with distinct glass microsphere contents: volume fractions of 20, 40 and 60%, sliding velocities of 1 and 3 m/s with 159 and 477 rpm were investigated. Other test variables included loads of 30 and 50 N, sliding distance of 1 and 3 km and two average nominal pressures of 0.21 and 0.35 MPa were the test parameters.[19]

Wear rate W_t was determined, using Equation 5.

$$W_t = (W_E - W_S) / (d_E - d_S) \tag{5}$$

Where E and S denoted the finishing and beginning of steady state wear. The friction coefficient μ was represented in Equation 6.

$$\mu = F_T / F_R \tag{6}$$

A graph was plotted against sliding distance *versus* height loss and another graph against sliding distance *versus* frictional force. An elevated height loss was obtained for pure resin, when compared with the HGM embedded epoxy-based SF at a 1000 m sliding distance. This implied that wear resistance was improved due to HGM fillers, whereas the frictional force exhibited a declining form with elevated time, when compared with the pure epoxy sample.

Therefore, with addition of HGM particles, applied normal load and distance for sliding, the rate of wear showed a decline trend. The glass microspheres of borosilicate offered resilience before getting broken into multiple smaller debris during wear. These small particles with the binder formed debris, which piled up within the broken HGM and reduced wear in the foam. When compared with other foams, neat epoxy exhibited greater friction coefficient (μ). μ can be decreased by increasing the sliding distance and the HGM filler loadings.[52] The post wear test of 60% HGM fillers in SF and higher magnification of debris is shown in Figures 12(a) and (b).
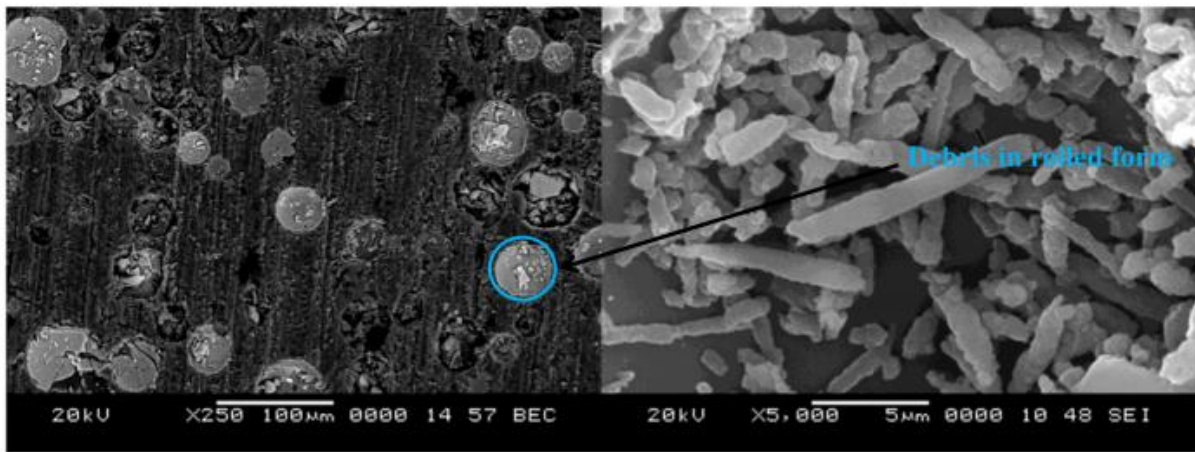
Figure 12. (a) Post wear test of 60% HGM fillers and (b) higher magnification of debris.[19]

(Reprinted with permission. Copyright 2019, IOP publishing).

6.8. Fracture Toughness. Quasi-static loading conditions were applied to SFs with different density HGMs for the fracture toughness test. The dimension of the each sample was $60.00 \times 12.70 \times 6.35$ mm³. Each sample was examined at a 5.00 mm/min crosshead speed and a 0.50 crack to width ratio (a/W).[12] The crack propagation, which was rapid at a particular point is called the critical stress intensity factor or fracture toughness (K_{IC}) and the values were calculated from Equation 7.

$$K_{IC} = Y.3PS \sqrt{a} / (2BW^2) \tag{7}$$

Where, $Y = 1.93 - 3.07 \, (a/W) + 14.53 \, (a/W)^2 - 25.11 \, (a/W)^3 + 25.80 \, (a/W)^4$ (8)

And P represented peak load, W denoted sample's width, S was the support span and a stood for the length of crack.

A graph was plotted between load and deflection. Due to negligible plastic deformation before fracture. It can be concluded from another graph plotted between K_{IC} *versus* volume of HGM fillers, the increasing volume fraction of HGM increased K_{IC}.[12] The maximum filler content increased due to a decreasing inter-particle dissociation and an increasing HGM microspheres that can be de-bonded from the matrix. The micro-cracks formed by de-bonding ahead of the crack tip initiated the propagation of cracks and minimized the fracture toughness, as the glass-bead content was added further.[53]

Ragosta et al.[54] studied the fracture toughness of epoxy/glass SFs as a function of strain rate, filler content and temperature. The density and the diameter range of the microspheres selected were 0.21 g/cc and 10 to 180 µm. The Charpy impact test was conducted at 1 m/s, 0.3 depth to weight ratio of 0.3 and a span of 48 mm. The tests were conducted at various temperatures ranging between room temperature to 80 ℃ and the graphs were plotted between load and energy against displacement time at each temperature. The fracture toughness or critical stress intensity factor was observed to be unaffected over temperature variation between room temperature and 80 ℃. The SEM micrographs of fractured surfaces showed that there were no clustering of microspheres and the features of deformation during the mechanism of fracture. The primary cracks were visible around the notch and the parabolic striations were considered to be secondary cracks in pure epoxy. On addition of HGM fillers of 5% volume, the amount of plastic deformation in the SF was comparatively less and the inter-crack development between microspheres caused brittle fracture, due to straightening of striations. This was the justification for the drop in fracture energy and fracture toughness. On increasing the volume

content to 15% of fillers, a crack pinning effect was evident, which enhanced the fracture toughness. The T_g increased with the microsphere concentration, but the fracture toughness was declined. This was due to the presence of more entanglements physically and restrictions in network mobility.

The stoichiometric fracture toughness of HGM/epoxy SF was studied by Kim et al.[55] with a microsphere density of 0.65 g/cc. The binder system consisted of epoxy blended with aliphatic amines, diethylene triamine and triethylenetetramine and the ratio of hardener to resin by volume was 1:5. An impact energy of 0.637 J, speed of cross heads at 5 and 0.5 mm/min with a height of drop of 0.38 mm were set as the test parameters of the universal testing machine to determine the fracture toughness. Despite of the pinning mechanism with an increase in micro-balloon content at low volume fractions, the specific fracture toughness did not improve drastically. The decline in fracture toughness was due to porous spaces present in the hollows of the fillers, which was not offset by the contribution from the pinning mechanism. Another cause for the loss in fracture toughness was that the areas of the fractured surface of the binders modified with HGM fillers did not appear to improve, when compared with unmodified epoxy binders.

Similarly, quasi-static loading conditions were applied to SFs with different density HGMs for the fracture toughness test by Wouterson et al.[56] The dimension of each sample was 60.00 × 12.70 × 6.35 mm³. It was examined at a 5.00 mm/min crosshead speed and a 0.50 a/W. The crack propagation became rapid the critical stress intensity factor or K_{IC} and the values were calculated from Equation 7.

Similarly, a graph was plotted between load and deflection. Due to negligible plastic deformation before fracture, it can be concluded from another graph plotted between K_{IC} versus volume of HGM fillers. With the increasing volume fraction of HGM, there was an increase in

K_{IC} values. The maximum filler content increased due to decreasing inter-particle dissociation and increasing HGM microspheres, which can be de-bonded from the matrix.[56] The micro-cracks formed by de-bonding ahead of the crack tip initiated the propagation of cracks and minimized the fracture toughness, as the glass-bead content was added further.

Zafran et al.[57] evaluated the methods to enhance the fracture toughness of SFs by varying the compounding without affecting the critical properties. The anhydride and amine were used as curing agents and elastomers in a desired proportion. The agents used for curing were nadic-methyl anhydride, hexahydrophthalic anhydride and bis(p-amino cyclohexyl methane). The conclusions made from the results obtained highlighted the possible of enhancing the fracture toughness of the SFs with anhydride by adding an elastomer. The SFs with bis (p-amino cyclohexyl methane) exhibited a higher fracture toughness than anhydride-based SFs in terms of both toughened and untoughened states. Another approach that yielded a 30% increase in toughness was by using cycloamine rather than using anhydride-based curing agents.

Wouterson et al.[56] selected three different micro-balloons, namely K15, K46 and 3M scotchlite with volume contents, ranging from 0 to 50% incorporated into epoxy matrix-SF and studied the fracture toughness through microstructures. The single-edge notched bend samples were subjected to a three-point bend under quasi-static loading in the fracture toughness assessment at a speed of cross head of 5 mm/min. The specification of the samples for fracture toughness assessment was $60.00 \times 12.7 \times 6.35$ mm³ that satisfied the plane strain conditions. The graph plotted between specific fracture toughness (K_{IC}/ρ) and volume percentage of microspheres showed that there was an increase in K_{IC}/ρ with an increase in volume content of the microsphere by 30%, due to the involvement of toughening mechanisms, such as a crack bowing mechanism from filler stiffening. However, the fracture toughness decreased beyond 30% volume of HGM fillers, due to a reduction in inter-particle separation between micro-balloons.

In addition, Maharsia et al.[58] investigated nano-clay hybrid SFs that were made of four types of hollow glass particles with different densities for fabrication. The foams were fabricated with a 35% volume fraction of binders and 65% HGM particles. Eight different types of nano-clay hybrid foams were prepared by combining two nano-clay particles of 2 and 5% in volume, respectively, with each microsphere type. It was observed that with the addition of 5% nano-clay particles, the increase in toughness was between 33 and 58% for high-density foams. The increase in specific strength and toughness was due to the presence of nano-clay fillers that enhanced the plasticization of the foam matrix.

The thermoplastic toughened epoxy with nano-clay reinforces hybrid SF was prepared by Rao et al.[59] with diglycidyl ether of bisphenol A (DGEBA) epoxy resin, diamino diphenyl sulfone (DDS), hydroxyl terminated polyether ether ketone having pendant methyl group (PEEKMOH), microspheres and nano-clay. The foam density was maintained between 0.6 to 0.72 g/cc and the fracture toughness was measured with respect to PEEKMOH concentration and clay. This research was focused on the fracture toughness measurement of SF based on epoxy/HGM filler with nanofillers toughened by PEEKMOH. An addition of 5% of clay fillers increased the fracture toughness by 26% and addition of 1% of PEEKMOH enhanced the fracture toughness by 43%. This was attributed to the synergistic outcome of enhanced interaction area along the area between binder, nano-clay fillers and PEEKMOH. The fracture toughness decreased with increased epoxy content, due to increased viscosity of binder which restricted the coalescence of binder domains. The specific fracture toughness initially increased up to 1% weight addition of clay fillers, but decreased beyond 1% due to the increased density of SFs.

6.9. Impact Resistance. The impact resistance is defined as the energy per unit area to fail the remaining ligament. They were notched to a a/W ratio of 0.25 with a hammer velocity of

3.46 m/s. Similarly, quasi-static loading conditions were applied to SsF with different density HGMs for the impact resistance test. The specification of the specimen was $60.00 \times 12.70 \times 6.35$ mm³, as examined at a 5.00 mm/min crosshead speed. Similar to the load *versus* volume percentage graph for fracture toughness, the load *versus* volume fraction graph for impact resistance proved the SFs to be brittle in nature.[12] Materials fractured catastrophically at a maximum load. Another graph was drawn with impact resistance and volume percentage. It was understood that the impact resistance reduced, due to the addition of micro-balloons. This reduction in values was not attributed to the type and volume fraction, but to the stress concentration induced that constrained the plastic flow of the polymer.[12] The fractured layer of the SF after dynamic impact is shown in Figure 13, where an arrow indicates the direction in which crack propagated.
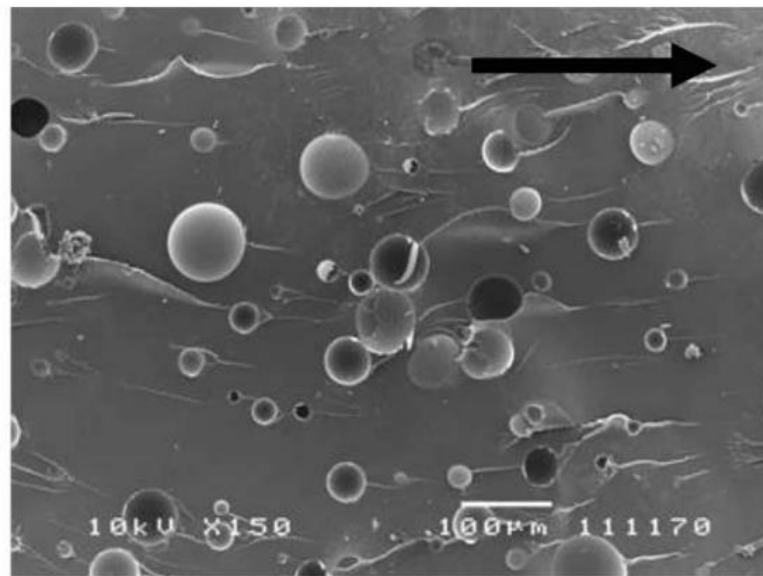

Figure 13. Fracture surface of SF after dynamic impact. The arrow indicates the direction of crack propagation.[4]

(Reprinted with permission. Copyright 2005, Elsevier).

6.10. Dielectric Properties. SFs made of epoxy/HGM possess a wide range of applications in electronic industries, where the materials used have lower dielectric constant. In this section, the effects of HGM fillers on the epoxy binder are reported. Generally, with the HGM fillers addition to the epoxy binder, there was a decline in density and elastic modulus values. The fabrication of this composite for analyzing its dielectric properties by mixing the epoxy resin and hardeners at a 4:1 mass ratio and mixing them manually by stirring for 5 minutes. Then, HGM fillers were added to the slurry and this was placed into a vacuum chamber for 3 minutes to eliminate voids.[60] Afterwards, the final mixture with reduced porosity was introduced into a cylindrical mold of 20×2 mm with polish and gold electrodes were sprayed evenly. The hardened composite was removed from the mold. Then, it was solidified for more than 24 hours at room temperature. It was observed that when the HGM content was below 20%, the slurry showed a relatively better fluidity. When the volume percentage increased by more than 20% weight, agglomeration took place and the viscosity became high. To maintain the fluidity, 3% weight of acetone was added to the mixture. Using an impedance analyzer, the dielectric properties of the composite foam were analyzed.

With its microstructural analysis, a few interesting results were obtained. The even dispersion of HGM particles in the epoxy binders was observed, as shown in Figure 14(a), and few broken HGM fillers were observed, as depicted in Figure 14 (b). This was caused during mechanical mixing. The addition of acetone content to 20% HGM fillers in the epoxy matrix improved the fluidity of the material. More pores were induced, due to the volatilization of the acetone in the composite. This caused the multilayer stacking structure of HGM fillers in the composite, as shown in Figure 14 (f). To obtain better interfacial adhesion between the matrix and reinforcement, HGM fillers maintained perfect spherical geometry.[60]
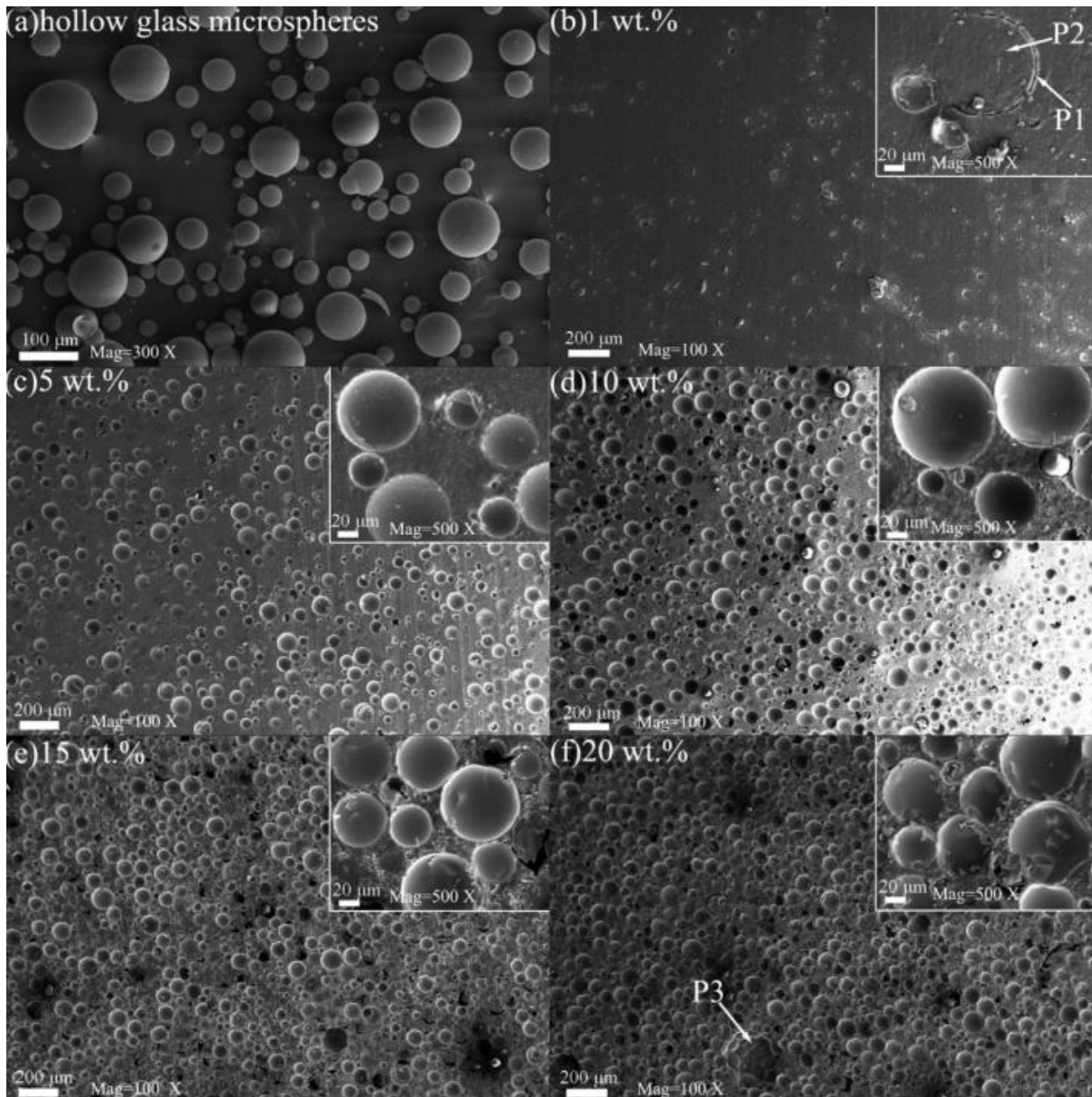
Figure 14. SEM micrographs, depicting (a) HGM fillers in epoxy matrix, (b) broken HGM fillers during mixing, (c) – (e) HGMs in the epoxy resin matrix become increasingly closer to each other with increasing HGM content and (f) stacking of HGM fillers caused by pores.[60]

(Reprinted with permission. Copyright 2019, Elsevier Ltd).

The contact electrode testing method with an impedance analyzer was adopted to study the dielectric properties of the material. The dielectric constant is defined as the medium capability

to store electrostatic energy in the electric field. The values were determined by using Equation 9.

$$\varepsilon_r = dC_p/A\varepsilon_0 \tag{9}$$

Where d, C_p and A were the length, capacitance, and electrode area of the sample, respectively, and ε_0 was the dielectric constant in vacuum. Two different frequency ranges were covered: 1 kHz to 1 MHz and 1 MHz to 10 MHz. It was evident that with increasing frequency, the dielectric constant showed a decline trend with increasing HGM fillers. The polarization of the material influenced the dielectric properties. Also, more the frequency caused less relaxation time. The dielectric constant of the sample was influenced by air gap in the frequency range from 1.0 kHz to 0.10 MHz and exhibited better frequency stability for frequencies greater than 0.1 MHz. This constant of the composite material was almost 87% lower than that of neat epoxy, when HGM particles in the composite aws 20% in weight. This was mainly due to the effects of large volume of voids and less dielectric constant of the HGM particles. A graph was plotted between dielectric loss *versus* frequency of the composite acoustic materials. The dielectric loss decreased with an addition of HGM content. For 20% of weight content of HGM fillers, the dielectric loss was 45% less than that of pure epoxy. This was the smallest in dielectric loss values.[60] Therefore, it was concluded that the dielectric loss and dielectric constant decreased with an increase in the HGM fillers and it showed a better frequency stability.

Baeriswyl et al.[61] studied the SFs with epoxy binders/hollow microspheres of ceramics, polymers and glass to determine the material with lower dielectric constant. The accumulation of interfacial water was tested up to 1000 hours of exposures to the humidity of 85% at 85 ºC. Through gravimetry and dielectric measurements, the water absorption capability was monitored. Impedance spectroscopy was carried out at frequency of 1 GHz. The results showed

that, when compared with the radius of the spheres, walls were not thin enough and therefore there was no significant decrease in the dielectric constant by ceramic microspheres. Significant decrease in dielectric properties were achieved with glass and phenolic micro-balloons, but the properties were deteriorated completely, because of the conduction-induced absorption of water around the spheres. The micro-balloons of acrylonitrile-vinylidene chloride in epoxy cured with amines yielded a lower dielectric constant, but the limitation was that it was easy to process.

The effect of absorption of water on the dielectric properties of glass/epoxy SFs with 3 mm thickness was investigated by Strauchs et al.[62] Three different HGMs used were: (i) untreated HGM particles, (ii) silane coated HGM particles and (iii) HGM particles with low alkali ion concentration, less than 0.40%. To promote the absorption of water, the temperature of deionized water in which the sample was stored was increased to 50 ^{o}C for 50 days of test period. The weights gained by the specimen when it was inside water were tabulated and analyzed to determine the increase in its weight, due to water ingress. The untreated SF with hollow glass spheres exhibited an increase in permittivity and loss factor during the testing time, while the SFs with silane coated and low alkali coated HGM fillers were insignificantly affected by absorption of water and therefore they can be used as an insulation material in outdoor applications.

Moreover, Schnettler et al.[63] studied the dielectric characteristics of SFs fabricated with the HGM filler incorporated epoxy binders of wall thickness of 1 μm and a mean diameter of 45 μm of the glass microsphere. During curing process, the viscosity of the liquid resin increased due to the addition of glass fillers. The uncured epoxy binders were blended with SiO_2 nano fillers to counteract the effect of viscosity before addition of the hollow micro-balloons. The loss factor and permittivity of samples were measured, using the setup that constituted of a circuit with device to be tested and a reference circuit with reference capacitor filled with 10

bar of N_2 and a loss factor less than 10^{-6}. Five different samples were tested, using the following measurement parameters; voltage and frequency of 1 kV and 50 Hz, respectively. Due to the presence of void in the glass particles, the permittivity of the foams reduced significantly, when compared with neat epoxy resin. The SiO_2 nano-particles possess increased permittivity, hence an addition of 0.5 to 2.5% of SiO_2 particles increased the permittivity of the overall material.

Four different types of HGM fillers, having 0.125–0.60 g/cc densities were filled in epoxy-binder and volume fraction of HGM fillers was varied from 0 to 60%. They were systematically investigated for dielectric properties. The bromine content of 19.0– 21.0% and the curing agent dicyandiamide and accelerator 2-methylimidazole were used as adjuvants by Wu et al.[64] The reflection loss and the dielectric constant were measured with an applied voltage of 500 mV and a frequency of 1 MHz, using an impedance analyzer. The dielectric loss and loss factor decreased with increasing the volume microsphere and/or decreasing the microsphere density. With increase in the temperature, dielectric constant (D_k) of the composite was observed to improve, while D_f increased initially and later decreased. Previously, Gupta et al.[57] measured D_k, dielectric loss (D_f) and electrical impedance as a function of temperature and frequency for four different SF compositions, in which the density and volume fraction of microspheres were 0.22 – 0.46 g/cc and 30% – 65%, respectively.

Additionally, semiconductor devices are packaged in epoxy-based polymer composites in order to reduce coefficient of thermal expansion. However, for high heat output devices, high thermal conductivity and low dielectric fillers are desired. In order to meet the need, Satapathy et al.[65] prepared a hybrid epoxy composited made of solid glass microsphere (SGM) with boron nitride ranging from 0 to 10 vol% in epoxy reinforced with 20 vol% of SGM, using hand lay-up method. The dielectric testing parameters were 500 mV of AC voltage and frequency range of 1 kHz to 1 MHz in an Elsier analyzer. The dielectric constant is the relative permittivity calculated from capacitance, using $D_k = Ct/\epsilon_0 A$, where t denoted disc thickness, ϵ_0 represented

vacuum dielectric constant; that is 8.85 x 10^{-12} farad per m and A stoood for area of disc. The dielectric characteristics involved different polarizations and the polarization rate was a function of temperature and frequency. At low frequency, the polarization possessed more time to complete. Hence, when the degree of polarization of a material is high and the dissipation of polarization is low, that is the dielectric constant decreases when the frequency increases. It was observed that D_k value declined with increase in boron nitride content in the glass/epoxy composite.

Strauchs[62] investigated the effect of modified interfaces by silane coating of HGM fillers on the electrical property of epoxy based SF. This silane coating process is known as silanization. It was done to enhance the adhesion quality between the HGM fillers and the epoxy binders. In this study, the impact of silanization on the electrical properties, higher breakdown field strength with respect to modified interface were investigated. The hollow micro-balloons of borosilicate with mean diameter of 40 µm, wall thickness of 0.88 µm and varied volume of micro-balloons from 20 to 50% were embedded in epoxy binders. The samples were connected on one side to an electrode of high voltage and measurement electrode with guard ring configuration on other side. The samples were coated with a conducting graphite member to achieve a better contact between the samples and the electrodes. The results showed that the silanization had no impact on relative permittivity and loss factor.

Winkel et al.[63] conducted an experiment on liquid nitrogen temperature (LNT) range to determine the dielectric parameters and the electric conductivity of SFs with micro-balloon diameter of 10 µm filled with SO_2. Epoxy resin and unsaturated polyester resin were chosen as binder materials with the average diameter of silanized HGM fillers as 45 µm and thickness of wall as 1 µm. Different samples were prepared with the 30 and 50% volume concentration of HGM fillers. SF was examined for relative permittivity, loss factor and electrical conductivity at liquid nitrogen condition, as these parameters have a high influence on generation of heat

within an electrical insulation. The conclusions were made from the test results that the dielectric parameters and electrical conductivity were not influenced by temperature between 65–77 K. The reason assumed was that above 65 K and below 140 K, SFs did not pass another secondary glass transition. For ambient and LNT conditions, the permittivity of the SFs was reduced by HGM fillers, due to relative permittivity of filled gas. It was evident that the permittivity and temperature were directly proportional, that is permittivity decreased with decreasing temperature, because at about 140 K, the molecular mobility was freeze. This was attributed to secondary glass transition of the binders.

From the material characterization of SF in the previous sections, it has been understood that this material provides an excellent combination of many structural properties that are essential for aerospace applications. These properties include, but are not limited to , light weight, low density, high T_g and low water absorption capability combined with better mechanical characteristics, which are better than the pure resin binder material. The low dielectric constant and very low loss tangent electrical properties of SFs have a relevance in RADAR absorbing materials in low observable or stealth technology in aircraft. In the subsequent sections, the basic parameters, terminologies of stealth technology, glass/epoxy-composite based material developments and the utilisation of syntactic cellular foam as a core in a sandwich layer of RADAR absorption materials (RAMs) to study their electromagnetic (EM) radiation absorbing properties, such as reflection loss to make an aircraft stealthier are addressed.

7. STEALTH TECHNOLOGY: BASIC TERMINOLOGIES

RADAR is a radio detection and ranging system that was first patented by Christian Hulsmeyre in 1904. It uses EM radiation (radio waves) to detect the location and movement of a structure.

Aircraft, spacecraft, guided missiles and weather formations are the targets. Invisibility approaches are contemporary topics in aeronautics, known as low observable technology or stealth technology. The composite RAMs used for stealth purposes are made of an insulating matrix (binder) and conductive reinforcement (fillers).[66] Object is detected when it gives the sign of its presence through sound, visual, smoke, radar, infrared and other signatures in the air.

The objective of stealth is to manage these signatures and reduce their revelation probability, using diverse sensors at a given range. This can be achieved firstly by optimizing the shape of aircraft. This is possible by scattering of incident EM waves into the environment. Secondly, using RADAR absorbing materials or structures that absorb incident radiation and convert it to heat energy.[67] Also, the working principle of RADAR reveals that EM radiation is transmitted from a transmitting antenna. This is done in the desired direction of the target through space, until the target is achieved.[68] When the EM pulses reach an object/structure, a part of the incident energy is absorbed, some portion is transmitted and the remaining part is reflected back and received by the receiving antenna of the RADAR system, as shown in Figure 15. The structures, including aircraft, spacecraft and missiles of interest are known targets. The unrelated objects, called clutters, which include buildings, sea and ground, are spotted by the target.[66] These clutters have been researched to filter out the actual targets.
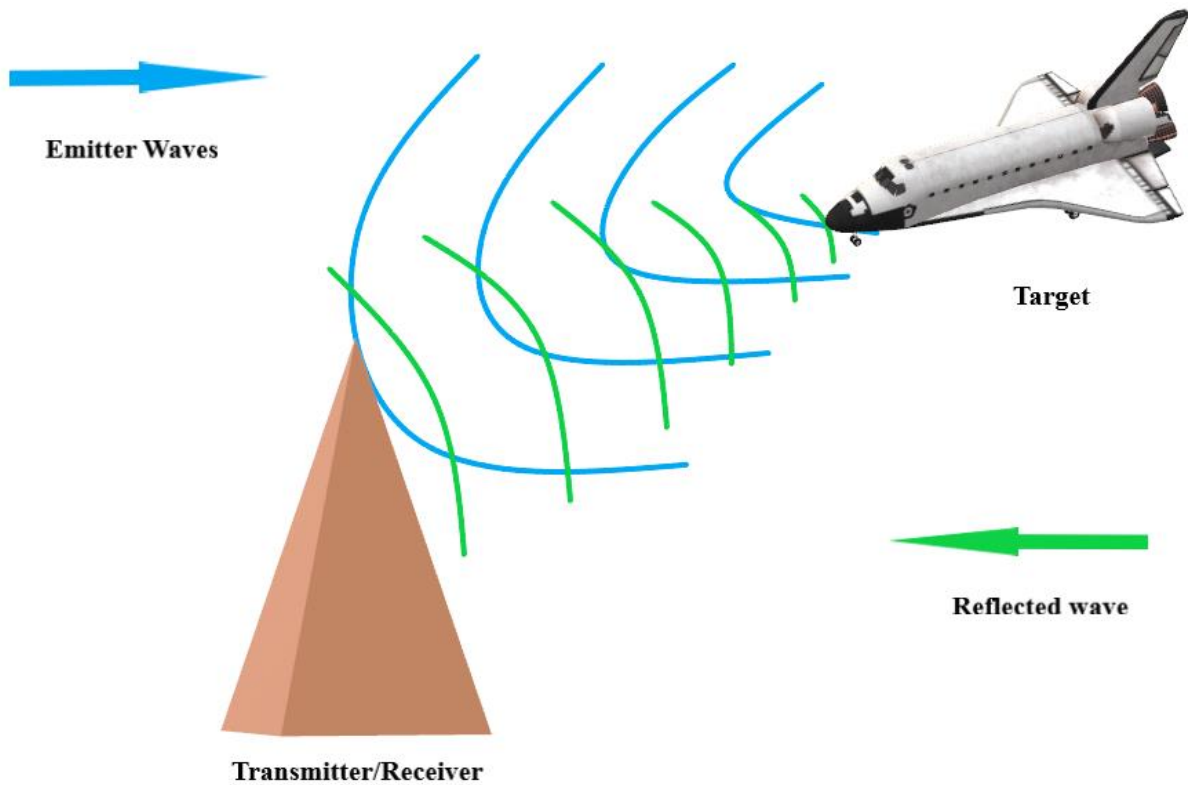
Figure 15. Working principle of RADAR.

The RADAR beam is generally conical in shape. Though, the radiance area is larger, only a considerable amount of incident wave is reflected again to the system. An antenna with a larger orifice is exclusively selected as the waves produced are narrow and reduce noise in the system. The interception ability of absorbed incident EM waves is usually greater. The probable gap between the target to be identified and the RADAR system is known as range (R) and it is calculated, using Equation 10. There are various parameters that can show the maximum detection range of RADAR. They are enumerated in this review.

$$R = Ct / 2 \tag{10}$$

Where c stands for the speed of light and t represents the time for the wave to reflect again to the system.

8. RADAR CROSS SECTION AND FACTORS AFFECTING RCS

The ratio of amount of the power reflected back to the amount of power incident on the structure is termed as the RADAR cross section. The range within which the target is observed is lowered with reduced RCS and *vice versa*.[69] In general, the RADAR absorbing structures (RASs) are fabricated using sheets of lossy dielectric materials and they are function of shape, frequency, aspect angle and polarization. The reflection loss ranging between -10 to -40 dB makes the aircraft stealthier, as shown in Figure 16.
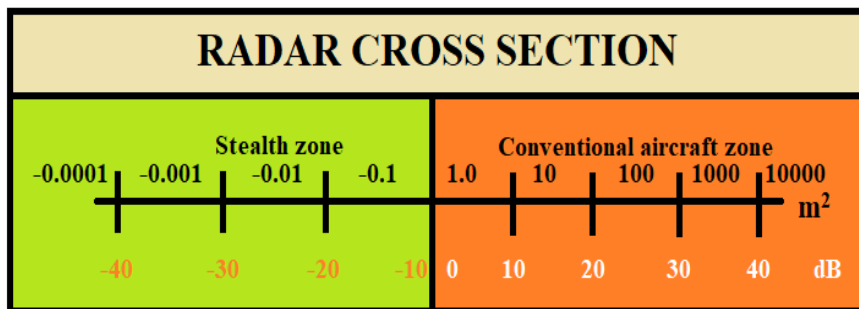
Figure 16. RADAR cross section scale.

The factors affecting the RADAR cross section (RCS) include[70]:

Target shape: For example, the EM waves from the parabolic shaped radomes redirects without any scattering to the radar system, but the EM waves are scattered in different directions in case of stealthy radomes with flat and sharp edges, thus results to reduction of RCS. Therefore, all modern stealth aircrafts are designed as flat with lots of sharp edges and corners.

Target material: The reflectivity of the aircraft material construction hugely impacts RCS; for example, metallic structures fully reflect the EM waves, leading to very high RCS. Hence, the metallic aero-structures are replaced with RAM for stealth improvement.

Radar frequency: The aircraft should be stealthy in the frequencies at which the radar operates. Broadband RAMs are recommended, as they possess ability to attenuate wide frequencies.

Orientation: The polarization of the outgoing and the incoming radiation depends on the orientation of the target.

9. RADAR ABSORPTION MATERIALS

RAMs are composite materials made up of a matrix material that acts as an insulating binder and magnetic fillers or conductive particles as reinforcements. The reflected pulse of EM waves is reduced when a considerable part of the incident radiation is absorbed by: (i) broadband RAMs by admitting the signals to reduce the intensity of the radiation and (ii) resonant RAMs, which generate internal reflection of incident waves. To minimize the reflected incident waves, the reflection coefficient r is calculated, using Equation (11).

$$R = (\eta_M - \eta_O) / (\eta_M + \eta_O) = (Z_M - Z_O)/(Z_M + Z_O) \tag{11}$$

Where, η_O, η_M and Z_O, Z_M are admittances and intrinsic impedances of the incident medium and reflecting substrate, respectively. From Equation (11), the reflection coefficient value is zero if the admittance of both mediums are the same, that is, when the impedance value of the incident and reflecting mediums are the same; there is no reflection.[66] The admittance and the intrinsic impedance of the medium are inversely proportional. The intrinsic impedance of free space is calculated, using Equation (12).

$$Z_{\text{free space}} = E/H = \sqrt{(\mu_o / \varepsilon_o)} \approx 377 \ \Omega \tag{12}$$

Where, E and H are the electric field and magnetic field factors, μ_o and ε_o are the permeability and permittivity of free space. Therefore, when the intrinsic impedance of the substrate is equivalent to 377 Ω, the reflection of radiation is zero. In order to achieve equivalent impedance

values of substrate equivalent to that of air, the surface of structures is coated with ferritic, magnetic or dielectric materials. Various factors that influence the energy absorbed by RAMs include coating thickness, incident wave angle and specific material characteristics. The dielectric lossy material is achieved by using materials with distinct impedance values. The lossy dielectrics are thicker, but less in weight, while the lossy magnetics are thin and heavy in nature.

10. TYPES OF RAMs/ RASs

The two important types of RAMs or RASs are impedance matching RAMs and resonant RAMs. The detailed descriptions of them are subsequently elucidated. Also, the types of these RAMs are later presented in Table 3.

10.1. Impedance Matching RAMs. The reflection of the incident signal from the target depends on the impedance values of the incident and the reflecting medium. The higher the difference in impedance, the higher the reflectivity from the structure to the system.[71] Therefore, it is important to note that the design criteria of the RASs for impedance values should match that of air of 377 Ω before it is gradually attenuated to 0 Ω at the rear surface. Since there are no sudden transition layers, the probability of large reflection is reduced.

10.2. Resonant RAMs/ RASs. In resonant RAMs, the impedance value cannot be matched due to low thickness. These RAMs work on the principle of destructive interference. When the microwave touches the front surface of the dielectric, a portion of the wave is reflected back to the radar system, some portion of the wave is absorbed by the dielectric and the remaining part is transmitted in various directions. The reflectivity of these RASs is studied by interpreting the permeability, permittivity and thickness of the layers.[72] The distance that the second wave travels extra causes it to be 180° out of phase with the initial wave by the time it appears from

the dielectric surface. When the second consecutive wave reaches the surface, both the waves cancel each other due to destructive interference, and as a result, there is no reflection on the radar system.[71]

Table 3. Various RAMs and their Working Principles

| Working principle	RAMs
Damp the EM wave energy (Impedance matching RAMs)	Tapered RAMs
	Pyramidal RAMs
	Matching layer RAMs
Destructive interference (Resonant RAMs)	Salisbury screen[73]
	Dallenbach RAMs[74]
	Jaumann layers RAMs[75]

11. FREE SPACE MEASUREMENT SYSTEM

The sample specimen is made of 150 x 150 mm cross section for the measurement of X-band free space permittivity. This system is composed of two X-band horn antennas up to 18 GHz for transmitting and receiving EM waves with a pair of spot-focusing lenses, a holder for specimen and a data-readable system, as depicted in Figure 17. To depreciate the diffraction fields, the lens is placed in front of antennas. From the antennas, the specimen holder is placed 300 mm. The sample is placed on the holder and the real and imaginary permittivity values are interpreted in frequency of 2 to 18 GHz.[69]
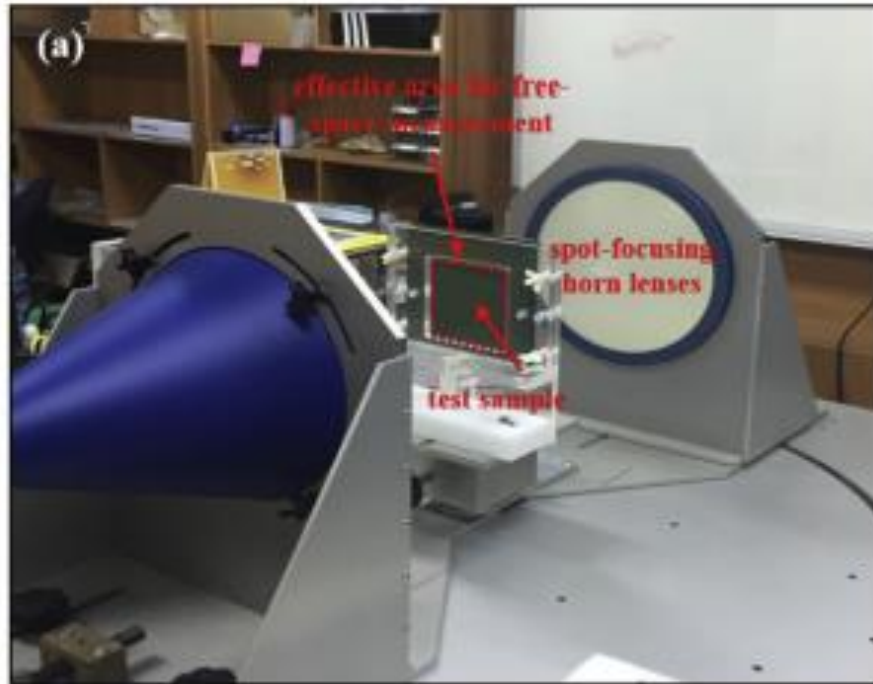
Figure 17. Free space permittivity measurement system.[76]

(Reprinted with permission. Copyright 2017, Elsevier Ltd).

Some errors are observed for lower thickness materials. For instance, in cases of optimal RAS, although the geometric compensation is applied to the waveguide. Therefore, measurement of reflection loss is done by using the RCS measurement technique in an anechoic chamber.[77] In the anechoic chamber, an antenna that transmits microwave is installed. Initially, a metal plate is placed on the chamber, known as the target (Figure 18). The reflected waves from the target are then measured. Again, the proper RAM is placed in the chamber as a target and the reflected wave from the RAM is taken, as shown in Figure 18.
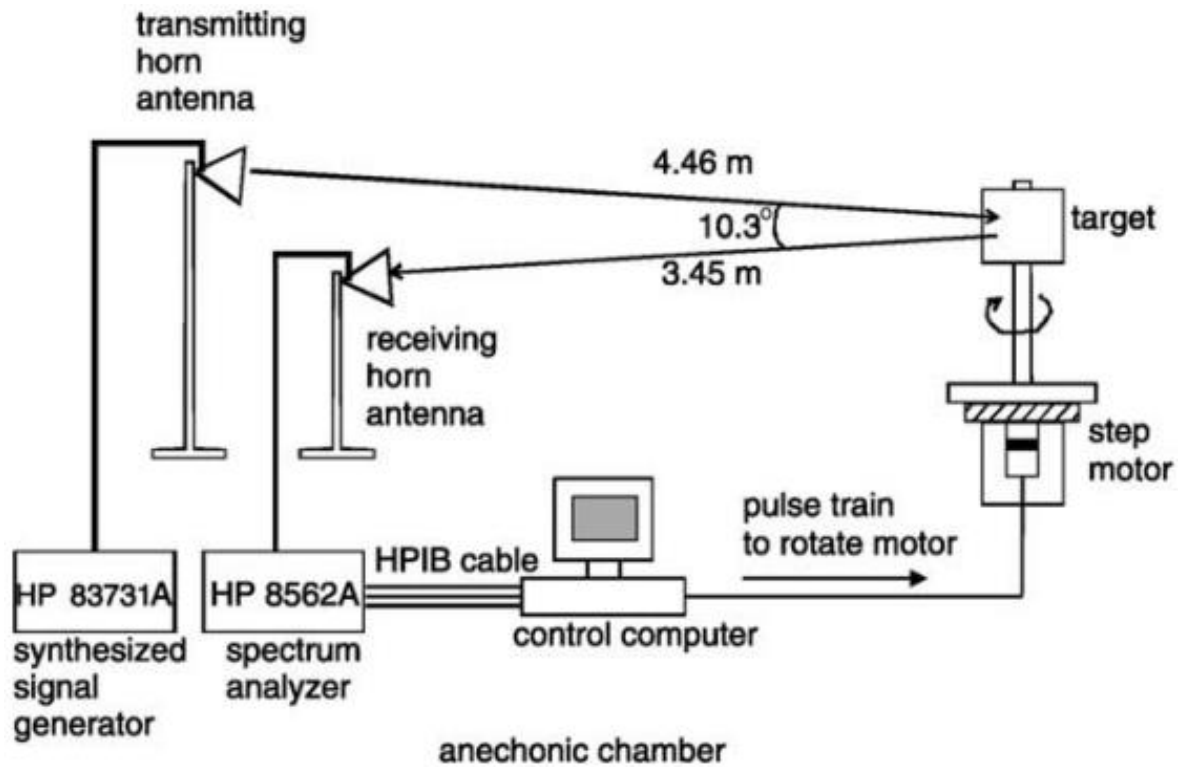
Figure 18. Reflection loss measurement in an anechoic chamber.[77]

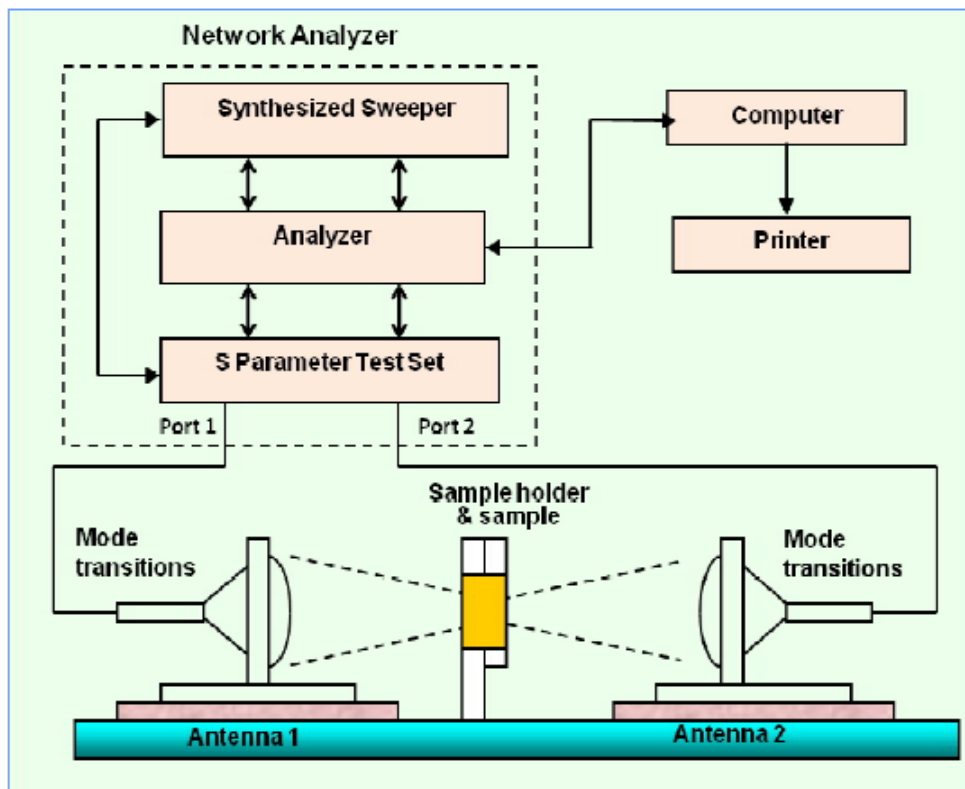(Reprinted with permission. Copyright 2004, Elsevier Ltd).

More also, the reflection loss of the RADAR absorbing material is the ratio of the two powers of reflected waves. Generally, a copper plate with high reflective power is utilized as a metal target. The accuracy in this technique is greater as the dimension of the specimen is comparatively higher than the waveguide method for measuring reflection loss. The accuracy of this method is detected by comparing the measured values and maximum RCS of conductive plate calculation, where the reflection is perfect. When the waves are incident normal to the surface, maximum RCS is achieved.

The materials for EM wave transparency to operate at various temperature should be selected in such a way that its dielectric properties should not vary in broad frequency regions with a low transmission loss of less than 1 dB is a desired for the RASs in microwave frequency region. Epoxy resin is generally used as the binder material to realize structural composites for

aircrafts. Their ease of handling, processability and low temperature curing make them widely used material ideally suited for such applications. Nevertheless, an operational temperature requirement of more than 250 °C limit the use of epoxy-based composites for radomes.[78]

Inamdar et al.[80] observed that properties of any composite to be transparent to EM waves is its lower dielectric constant (permittivity, ε) and in specific, low imaginary permittivity (ε''), and low loss tangent (tan δ). However, the dielectric constant increases with increasing temperature beyond T_g, because of increased segmental mobility. It also increases with moisture content that leads to increase in heat content in composites, which reduces EM transparency.[81] Hence, for high-speed aircraft radomes, it is mandatory to use high-temperature capable, highly tough, low loss composite materials with low moisture uptake[82], as illustrated in Figure 19.

Figure 19. Block diagram of free space measurement system.[79]

(Reprinted with permission. Copyright 2016, IEEE publications).

12. ENHANCEMENT OF ABSORBING PROPERTIES OF GLASS/EPOXY COMPOSITES

In a study, Mishra et al.[69] compared the microwave behavior of glass/epoxy composites with: (i) magnetic fillers and (ii) carbon-based fillers. A wet lay-up method was adopted to cure the composite with a minimum density, low thickness and a bandwidth of 2-18 GHz. The free space measurement was carried out for reflection measurement of a sample of 150 x 150 mm in dimension. The measured reflection loss showed that the reflectivity of the carbon filled composite was low and less than -10 dB for a bandwidth frequency range of 4-12 GHz, when compared with the composite blended with magnetic fillers, the loss was observed to be 10 dB at frequency range of 4 to 10 GHz.

In another research, conductive CB was blended with the glass/epoxy composite and the EM wave absorbing properties were investigated. The CB additive initiated the dielectric loss. The specimen was fabricated to 10.1 x 22.9 mm, inserted into the wave guide and a network analyzer was used to measure the S-parameters to calculate the real and imaginary permittivity of the specimen.[77] This procedure was repeated for specimens with varying CB contents. A graph was plotted between frequency and permittivity. The results showed that the permittivity of the sample with 15 and 20% carbon fraction cannot be measured, due to the uneven dispersion of CB particles. This was because the pre-mixed binder resin produced a high viscosity during manufacturing. The gaps between wave guide and sample were expected to be sealed properly as the gaps between them decreased the transmissivity. The graph also indicated that the sample with 10% of CB reflected 47% of EM waves. Therefore, samples with a low proportion of CB produced a better performance and can be considered for RAS.

A double-layer radar absorbing material made of epoxy/E-glass fabric layers was ideally intended to have a broad bandwidth in the region of X-band, as reported by Park et al.[83] A pure

E-glass fabric/epoxy composite laminate was the first layer and carbon nanocomposite laminate acted as the second layer. The fillers included carbon nanomaterials, containing CB, CNT and CNF, were used. To determine the optimal thicknesses of the consecutive layers, numerical models of the real and imaginary permittivity of carbon nanocomposites were incorporated into the design process. The locations of the two peaks in the frequency domain was varied to design the RADAR absorbing structures with different absorbing performances. Additionally, the influences of the EM properties of each carbon nanomaterial on the thickness and the absorbing performance were analyzed. The carbon fillers and the composite thickness were used explicitly as optimization variables by adopting the semi-empirical model proposed by Kim et al.[84] Compared with absorbers made of the CNFs and CNTs, the absorber prepared with CB composite had a narrower bandwidth. The large real permittivity (ε_r') was more substantial than the imaginary permittivity to acquire thin sheets and good peak separation for a huge absorbing bandwidth. The -10 dB bandwidth and the thickness were 7.7 GHz and 4.090 mm, owing to the large ε_r' of the CNF composites and 7.4 GHz and 4.277 mm for CNT composites. The -10 dB bandwidth and absorber thickness for the CB-composite were 7.5 GHz and 4.680 mm, respectively. The RAMs exhibited great mechanical behavior, absorption properties and less interference, making them useful for EM interference shielding and radar absorption. Ashraf et al.[85] investigated into the EM waves attenuation by adding different carbon-based absorbers in glass/epoxy composites. The lossy fillers utilized included short carbon fibers (CFs), such as CB and MWCNTs. The vacuum assisted resin infusion technique was uesd to manufacture the specimens with uniform thickness and minimum porosity. The samples were tested, using free space measurement technique for reflection loss and complex permittivity. Novel designed high strength CFs were fabricated and trimmed into small strands. Then, they were dispersed in the layers of glass fibers uniformly. Thus, fabricated structure had 8 to 24 layers of glass fiber with incorporated CF strands. The permeability, permittivity,

dielectric loss and reflection loss were investigated in the study. The best results were obtained with short CFs among the lossy components used with a maximum reflection loss of around 24 dB; approximately 99% absorption. Moreover, best possible thickness was achieved with 16 layers of glass fibers. Greater number of layers provided some absorption nearly 10 dB, which was 90% absorption, whereas there was no absorption obtained using a smaller number of layers and the structure was transparent. CNTs and CB showed transparency as their number of layers was low.

Furthermore, a single-layered and double-layered wave-absorbing sheathing with absorbents comprised of CB with epoxy as binder was prepared by Mehdizadeh et al.[86] to prevent EM interference. SEM and atomic force microscope were utilised to determine the morphologies of CB/epoxy-based composites. The CB filler exhibited polyaromatic behaviour, as described with X-ray diffraction technique. The microwave parameters of CB were measured in the X-band frequency range by transmission/reflection, and the reflection loss mechanisms of the particles were discussed. The EM absorption properties of the coatings were observed to measure reflection loss using arch method and the effects of CB ratio, thickness and double-layer on the EM absorption properties were reported. With increasing CB ratio or thickness, the frequency of absorption bands shifted towards the lower frequency range. Therefore, by varying the percentage of CB present in the composites, the wave-absorbing coating could be applied in desired frequency range. Besides, for the specimens with thickness of 3 mm, by adding CB content, the absorption bandwidth (RL < 4 dB) can be enhanced especially for the double-layered specimen with CB ratio of 7 added to 10 wt.%, the absorption bandwidth attained -32.1 GHz.

Kim et al.[87] investigated into the EM absorbing characteristics of a two-layer composite laminate of CF/epoxy composite plate with CB impregnated rubber sheet. Using a network analyzer and a coaxial waveguide, real and imaginary permittivity and permeability of the

composites were measured in C-band and X-band frequencies between 4 to 12 GHz by reflection/transmission method. By varying the amount of CB present in the rubber composite, the permittivity can be controlled. The dielectric constant and dielectric loss values were observed to be high in the CF material. Optimization of EM absorption was performed for the double-layered RAM on the basis of transmission line theory. It was observed that the EM absorbance of CB-absorbing layer was strongly impacted by the electrical characteristics of the CF/polymer composite. An eminently absorptive RAM can be designed by laminating the CB and CF composites on the basis of transmission line theory. For this double-layered material with the rubber sheet containing 10% content of CB, the maximum EM absorption of 30 dB was indicated at 10 GHz.[87]

Moreover, Sang-Eui Lee et al.[88] designed a RADAR absorbing material (RAS) that operated in X-band frequency to determine the load-bearing capacity and microwave absorbing characteristics. MWCNTs were incorporated as fillers in glass/epoxy composites, which exhibited excellent specific stiffness and strength, to induce dielectric loss. The microstructural analysis and the complex permittivity of the structure confirmed that the components were suitable to be used as RAMs. A genetic algorithm (GA) and a theory of reflection/transmission of microwaves were implemented to design an optimal RAM with MWCNT-loaded composite material. With varying number of plies and the contents of MWCNT, the thickness per ply of the material tended to vary. A program was coded to predict the reflection loss of a multi-layered RAS for normal incident EM waves in the frequency between 8.2 – 12.4 GHz. To design the RAM, a code was linked with the genetic algorithm. The microstructural detailing revealed that a high dielectric loss was induced, as confirmed by permittivity measurements, due to the uneven dispersion of MWCNTs. Based on this result, the designed double-layered RAM recorded 90% absorption of microwaves for the entire X-band frequency of 8 - 12 GHz.

Kim et al.[90] fabricated a RAM as a sandwich structure made up of nanocomposites, CF/epoxy material and polyvinyl chloride (PVC) foam. The nanocomposite made up of E-glass fiber, epoxy binder and CNT was adhesively coupled to the external surface of the sandwich layers in order to absorb microwaves. The CF/epoxy composite acted as both reflection plate of incident microwaves and a load bearing material. The microwave absorbing characteristics were assessed by the free space measurement system. The bonding properties between nanocomposites and CF/epoxy materials were also analyzed, using the free space measurement system. The dielectric characteristics of the nanocomposites were measured as a function of weight percentage of CNTs.[89] The result showed that at thickness of 2.52 mm and weight content of 3% of CNTs, the absorbing bandwidth of -10 dB was 3.3 GHz (8.2 – 11.5 GHz). The maximum microwave absorption rate was 97% and the minimum rate was observed to be 84%. The peel strength of the composite was about 3.8 kN/m. Finally, an exceptional composite sandwich material that can absorb incident microwaves more than 90% in the X-band frequency range of 8-12 GHz and that has better bonding properties between the nanocomposite and the reflection sheet was suggested.[90]

Also, the addition of micro or nano-fillers in order to optimize the mechanical and EM properties of epoxy-based composites has become a common practice. The CNT possess excellent stiffness, thermal conductivity, electrical capacity and thermal stability along with greater EM wave absorption capability. Silva et al.[91] studied the microwave absorption characteristics and dynamic-mechanical response of glass fiber/epoxy composites in which CNTs were embedded. A novel procedure to distribute and deposit CNT onto glass fibers evenly was developed to achieve an overall content of CNT up to 4.15 wt.% in the composite. This was done by adopting resin transfer molding (RTM) to fabricate thinner materials with EM wave attenuation properties in the X-band region and CNT as a microwave absorbing centres. The microwave absorption by the composites recorded an increasing trend for higher

CNT content (up to 2.0 wt.%), reaching a maximum of approximately -18.3 dB (98.5% of absorption). This was obtained using a comparatively low cost glass fiber and very thin polymer composite material of 2.2 mm. Therefore, the produced composites exhibited a great potential to be used as RASs.

The fillers added to the composite can be semi-conducting materials, such as carbon-based inclusions in form of powders, flakes, tubes, fibers or dielectric materials with high permittivity, including oxides and titanates. Others are ferro or ferri-magnetic materials with high permeability or combination of both magnetic and dielectric materials.[92] From the aforementioned studies, it was evident that the utilisation of CFs was limited, because of its highly conductive nature in stealthy structures, since it reflected the incident EM waves back to the receiver completely, rendering complete radar visibility.[70]

In addition, a new absorbing material was fabricated by Nam et al.[76] from glass/epoxy materials. The glass was coated with a thin conductive layer of nickel (Ni), which produced an excellent absorbing performance and a reflectivity loss of 90% in the X-band region. The fabrication of this RAS included the following process. The Ni-coated glass fabric was layered with a glass/epoxy prepreg. The appropriate design thickness was selected. The layering was done using a hand lay-up method along with the curing accessories and was handled by the number of plies to be layered. On the mold, a release film and a perforated film was placed over it and peel-ply were placed on the layered sample after the lay-up of the prepreg and Ni-coated glass particles. The layered Ni-coated glass fabric and glass/epoxy prepreg together with breathers were vacuum bagged and cured subsequently in an autoclave. The curing cycle at beginning was maintained for 30 minutes at 80 °C, and the next cycle was held for 120 minutes at 130 °C. The cured composites were then made into desired specifications to measure the return loss for the X-band of frequency ranging between 8 to 12 GHz with a free-space measurement system, as shown in Figure 20.
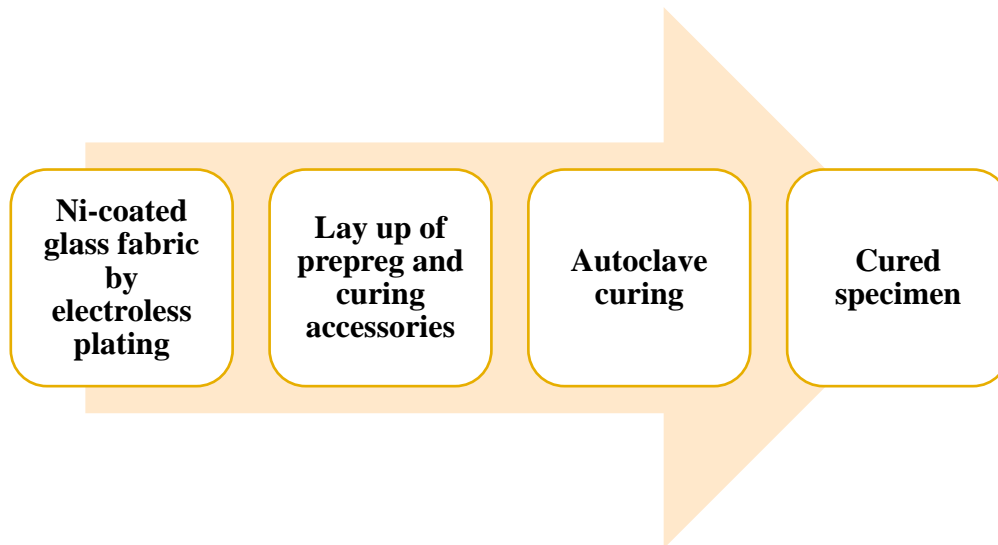
Figure 20. Fabrication of proposed Ni-coated microwave, absorbing structure by electroless plating.

This was much more effective than blending the composites with CB, CF or CNTs.[76] Three samples with varying thicknesses of a one layered and two double-layered absorbers were considered. The electroless plating method was performed to produce a thin layer of Ni coating over the dielectric glass fibers, whose composition was analyzed by energy dispersive spectroscopy (EDS). The fabricated specimen was measured for permittivity in the free space system. A cole-cole graph was plotted with real (x-axis) and imaginary (y-axis) permittivity at 10 GHz for a particular design thickness.[93] It was observed that the increase in permittivity was due to increasing Ni content. The electroless plating improved the interfacial bonding between the binders and the reinforcement by creating active sites. The conclusions from the final results were that the double slab absorbers possessed excellent absorbing performance with a reflection loss below 10 dB between 8.5 and 11.5 GHz, while the single slab absorber did not match the simulation results.

Moving forward, reduction in weight of the parts coupled with effective performance of the system as well as fuel economy and improved payload capacity are desired in aerospace applications. The tailorable properties of composite materials have provided designer

opportunity to alter their properties, such as strength, modulus, fracture toughness and thermal stability, among others. Epoxy binder-based composites with fibers or reinforcements of high strength, such as carbon/glass have been major class of materials that are suitable for such special applications.[94] However, the epoxy-based systems have various limitations. These include, but are not limited to, excessive absorption of water and residual stresses, leading to initiation of micro-cracks when thermally cycled.[92] Also, the maximum service temperature of these epoxy systems is around 177 °C. The temperature is restricted to 149 °C in moist conditions. Hence, composite materials, such as epoxy/glass SFs exhibit high service temperature, improved toughness, dielectric characteristics and less water absorption with high strength-to-weight ratio and stiffness-to-weight ratio properties.[95]

Various studies have been carried out to overcome EM interference by inducting ferrite absorbers, but the weight and density increase more than the desired level with a narrow bandwidth in absorption.[96] Also, several non-magnetic particle-based EM absorbers have been proposed, but the thickness of the materials are more than critical value and suffer. This is because their reflection loss is less than 10 dB, a limitation for airborne application.[97] The bulky nature and greater thickness of pyramidal shape absorbers limit them, even though they absorb EM radiation in a wider range. The SF supports the RASs with low weight, less density, better mechanical properties and an excellent EM attenuation property.

Kumar et al.[79] proposed a RAM based on a sandwich structure with SF as the core structure to reduce the density for the X-band from 8.4 to 12.8 GHz and Ku band with frequency region from12.8 to 18.4 GHz. The composite was fabricated with an impedance hierarchy for EM attenuation properties above X and Ku band frequency regions and the mechanical characterization was verified. In this research, the intended broadband EM absorbing materials were made up of dielectrics, such as CB and CFs for sandwich RAMs. The lower thickness and density of the designed structure reduced the RADAR cross section. The fabrication of the

sandwich RAS was based on a cladded model. The cladded structure was made in such a way that the EM radiation was completely attenuated and not radiated, due to the terminating layers. A perfect electric conductor (PEC), including CB was used as the terminating layer and the permittivity and thickness of the laminates were designed to permit maximum attenuation of EM waves in the X and Ku band regions. The hardener (Aradur-5052), the matrix (epoxy resin) and the glass fabric reinforcement were cured at room temperature and the SF acted as a core material co-cured with CB, aluminum flakes and CF as absorbing fillers at various fractions, as shown in Figure 21.

Figure 21. Sandwiched RAS composite.[79]

(Reprinted with permission. Copyright 2016, IEEE).

Epoxy resin with one ply of carbon fabric was considered to be PEC that acted as the microwave reflecting layer. Three plies of glass fabric reinforced epoxy matrix modified with absorbing fillers at various proportions acted as a functional layer, as previously shown in Figure 21. Finally, the cladded RAM was fabricated, using a vacuum bagging process. The RAM wsa characterized by reflection loss and permittivity values, using free space permittivity measurement. Thru-reflect line calibration was done, followed by measurement of real and imaginary permittivity and then the reflection loss, R_L was calculated, using Equation 13.

$$R_L = 20 \log \left[\frac{Zin - Zout}{Zout} \right] \tag{13}$$

Where, Z_{in} and Z_{out} (or Z_o) were the input and free space characteristic impedance, respectively, and:

$$Z_{in} = Z_0 \sqrt{\frac{\mu_r^*}{\varepsilon_r^*}} \tanh(j \frac{2\pi fd}{c} \sqrt{\mu_r^* \varepsilon_r^*}) \tag{14}$$

Where f, d and c are frequency of microwave, thickness of the absorber and velocity of the EM waves in free space, respectively.

Also, complex permittivity, $\mu_r^* = \mu_r' - j\mu_r$ (15)

Similarly, complex permeability, $\varepsilon_r^* = \varepsilon_r' - \varepsilon_r$ (16)

Where ε_r' and ε_r are real and imaginary permittivity, respectively.

The material being dielectric, $\mu_r' = 1$ and $\mu_r = 0$ and the reflection loss was calculated based on Equation (14). This sandwich structure based on transmission line theory and the vacuum bagging process resulted to a minimal reflection loss of 10 dB in the frequency bandwidth of 8.2 to 18.4 GHz, as shown in Figure 22. The composite structure exhibited very good EM radiation absorbing capabilities with a desired lower reflection loss of less than 10 dB, which showed its potential implementation in the reduction of RCS in stealth technology.
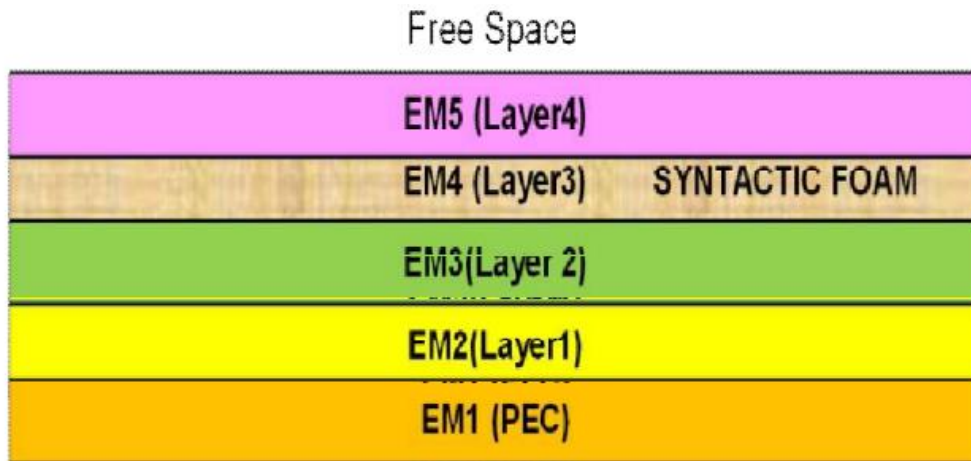
Figure 22. Schematic representation of a sandwich RAM.[79]

(Reprinted with permission. Copyright 2016, IEEE).

13. MICROWAVE–MATERIAL INTERACTION FOR REFLECTION LOSS

The irregular placements of the CNF in the epoxy matrix are presented in Figure 23 to understand the EM radiation storage and loss mechanism with the help of ε_r' and ε_r. The CNF/epoxy nanocomposites backed by a metallic conductor contain various dipolar groups coupled via a bond between them. The permittivity of the dielectric material and the thickness of the panel determine the absorbing ability of the composite. Over 90% of the composite is filled with absorbing foam. The absorbing performance is weakened to a relatively small degree by the glass fiber reinforced plastic lattice material.[98] A proper microwave-material interaction model is depicted in Figure 23.
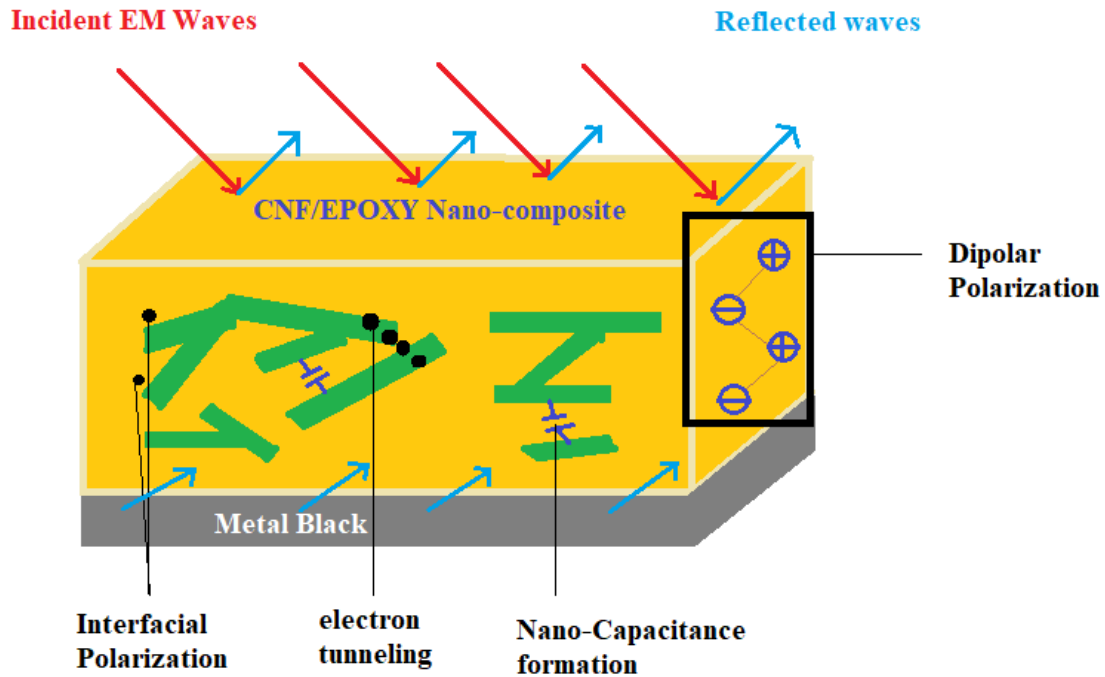
Figure 23. Microwave-material interaction model.

The factors that affect ε_r' with increasing CNF fractions[99] include:

(1) Interfacial polarization: The physical and chemical behaviors of the nanocomposites are affected by the interaction between the matrix and reinforcements at the interface region. Interfacial charges accumulate at this region based on the conductivity at the interface.[100]

Higher ε_r' is eventuated as the CNF concentration increases and large interfacial surfaces are induced, due to the wider surface area of CNF particles.

(2) Formation of nano-capacitors between the conductive nano CNFs. The random arrangement of CNFs in the matrix possesses cylindrical geometry either crossed paths or parallel with each other and exhibits anisotropic properties. There is no capacitance observed in cross paths, but a dominant capacitance, that is, storage of electrical energy is observed in the parallel arrangement of CNFs. Therefore, the ε_r' improves with higher CNF concentration, because there is a higher probability in the formation of nano-capacitor. The relationship between ε_r' and C is represented in Equation (17).

$$C = (A \, \varepsilon_r')/d \tag{17}$$

Where A represents the surface area of CNF and d is the thickness of the epoxy layer between two nano fibers.

(3) Dipolar polarization in the epoxy nano composite: The dipoles that exist in the matrix are polarized when they interact with the microwave energy. With respect to the excited frequency, they oscillate and can store energy.[100]

The factors that influence the ε_r include: (i) resistance of conducting CNFs. The values of R_c are influenced by intrinsic resistivity, length of the fiber and diameter of CNF. Since CNFs conduct electric charges, values of R_c are assumed to be low. R_c values are based on the intrinsic properties. Therefore, they are not affected by the concentration of CNFs. (ii) resistance to electron tunneling. With applied microwave, electrons can travel through layers of the matrix, causing a conducting path with a tunnel resistance, R_t. The values of R_t are influenced by the epoxy layer thickness between CNFs. R_t decreases with increased contact between them and lowered thickness of the epoxy matrix at high CNF concentration. Hence, the overall tunnel resistance, R_T decreases and *vice versa*.[99] Conductivity increases with CNF concentration, resulting to greater values of ε_r. EM wave loss is observed, due to interfacial polarization and dipolar relaxation. It is observed that, when the frequency increases at higher fractions of CNF, the values of ε_r' and ε_r are reduced significantly, as the polarization effects are unable to respond due to inertial effects.

14. CONCLUDING REMARKS

Syntactic cellular foam is a lightweight composite. The addition of HGM fillers to the matrix enhanced the performance of the composite significantly. The tailorable properties of SF made them dominant in various fields. The structural morphology of SF has been discussed in this

review along with its properties and characterization. The foams processed with the degassing method evidently reduced the matrix porosity and the increased volume fraction of HGM fillers gradually decreased the density of the composite.

In addition, the tensile test established that the tensile characteristics of foam increased with HGM fillers, due to better interfacial interaction between the matrix and the hollow microspheres. The compressive properties can be improved by two methods: either by reducing the volume fraction of microspheres or by calculating the radius ratio (η) as a function of inner and outer radii, because decrease in η increases the compressive properties. The volume fraction of HGM fillers has a dominant effect, but wall thickness was less prominent on T_g. Due to the interfacial reactions between the matrix and the fillers, the T_g of all other foams was less when compared with pure resin. Pure epoxy exhibited wear, whereas the wear rate decreased with the inclusion of HGM fillers. With an increase in the HGM fillers, the coefficient of friction decreased.

Besides, the fracture features of all varieties of SFs were identical. During compression, shear cracks were formed initially, which propagated vertically and then fractured. By adding HGM particles to the epoxy matrix, fracture toughness increased, but there was a decline in impact resistance. The dielectric loss and dielectric constant decreased with an increase in the HGM fillers and it showed a better frequency stability. The distinct or unique properties and their utilisation in various fields for effective and efficient performance have also been reported. From the above material characterization, it was observed that the SF has impressive mechanical behavior as well as high strength-to-weight ratio, low density, low water absorption capability and high T_g combined with high structural properties that are desired for aerospace applications.

Moreover, the SFs possessed low dielectric constant and very low loss tangent electric properties, enabling their utilization as RADAR absorbing materials to make an aircraft stealthier. Therefore, relevance of various terms and parameters in stealth technology, such as RADAR cross section, reflection loss and the working principle of RADAR were reviewed. The RADAR absorbing materials, their classifications and few processes that enhance their absorbing performance by adding filler materials to improve their reflection loss have been well elucidated. The reflection loss and other EM wave absorption of a sandwich layer that used SF as a core material to make the aircraft stealthier were studied. The concept of how other parameters, such as thickness of the layers and permittivity of the dielectric material affected the performance has been reported within the scope of this compendious review. For instance, variation of absorbing performance and reflection loss for glass/epoxy composites when blended with magnetic and carbon fillers: CFs, CB and CNTs has been extensively discussed. A RAS with syntactic cellular foam as a core material was studied. It was observed that this material provided better mechanical properties with low RCS and excellent EM attenuation property, hence making the aircraft stealthier. Finally, the microwave-material interaction model and its influencing factors have been included in this present study. Therefore, this informative review has potential to contribute relevant and detailed knowledge of innovative materials for advancement of both aerospace and military/defense sectors.

ACKNOWLEDGEMENTS

review article to Dr. Nikhil Gupta, Professor, New York University Tandon School of Engineering Department of Mechanical and Aerospace Engineering.

REFERENCES

(1)   T. C. Lin, N. Gupta, and A. Talalayev, Thermoanalytical characterization of epoxy matrix-glass microballoon syntactic foams, *J. Mater. Sci.*, 44, 6, 1520–1527, 2009, doi: 10.1007/s10853-008-3074-3.

(2)   S. Sankaran, K. R. Sekhar, G. Raju, and M. N. J. Kumar, Characterization of epoxy syntactic foams by dynamic mechanical analysis, *J. Mater. Sci.*, 41, 13, 4041–4046, 2006, doi: 10.1007/s10853-006-7607-3.

(3)   V. S. Le *et al.*, Mechanical properties of geopolymer foam at high temperature, *Sci. Eng. Compos. Mater.*, 27, 1, 129–138, 2020, doi: 10.1515/secm-2020-0013.

(4)   E. M. Wouterson, F. Y. C. Boey, X. Hu, and S.-C. Wong, Specific properties and fracture toughness of syntactic foam: Effect of foam microstructures, 2005, doi: 10.1016/j.compscitech.2005.03.012.

(5)   L. O. Afolabi *et al.*, Syntactic foams formulations, production techniques, and industry applications: A review, *J. Mater. Res. Technol.*, 9, 5, 10698–10718, 2020, doi: 10.1016/j.jmrt.2020.07.074.

(6)   N. Gupta, E. Woldesenbet, and Kishore, Compressive fracture features of syntactic foams-microscopic examination, *J. Mater. Sci.*, 37, 15, 3199–3209, 2002, doi: 10.1023/A:1016166529841.

(7)   M. R. Doddamani and S. M. Kulkarni, Dynamic response of fly ash reinforced functionally graded rubber composite sandwiches - A Taguchi approach, 3, 1, 166–182, 2011.

(8)   G. Microballoons, Enhancing the ignition , hardness and compressive response of

magnesium by reinforcing with hollow, 2017, doi: 10.3390/ma10090997.

(9)   B. Zhang, Z. Fan, S. Hu, Z. Shen, and H. Ma, Mechanical response of the fly ash cenospheres/polyurethane syntactic foams fabricated through infiltration process, *Constr. Build. Mater.*, 206, 552–559, 2019, doi: 10.1016/j.conbuildmat.2019.02.047.

(10)   P. k R. Nikhil Gupta, Metal matrix syntactic foams, in *Metal matrix syntactic foam: Processing, Microstructure, Properties, and Application*, DEStech Publications, 2015, p. 351.

(11)   D. Pont, A. F. Tegeler, O. Fallon, and L. Tracy, United States Patent (19), 19, 1997.

(12)   E. M. Wouterson, F. Y. C. Boey, X. Hu, and S. C. Wong, Fracture and impact toughness of syntactic foam, *J. Cell. Plast.*, 40, 2, 145–154, 2004, doi: 10.1177/0021955X04041960.

(13)   N. Gupta and E. Woldesenbet, Microballoon wall thickness effects on properties of syntactic foams, *J. Cell. Plast.*, 40, 6, 461–480, 2004, doi: 10.1177/0021955X04048421.

(14)   S. E. Zeltmann, B. Chen, and N. Gupta, Thermal expansion and dynamic mechanical analysis of epoxy matrix–borosilicate glass hollow particle syntactic foams, *J. Cell. Plast.*, 54, 3, 463–481, 2018, doi: 10.1177/0021955X17691566.

(15)   H. S. Kim and P. Plubrai, Manufacturing and failure mechanisms of syntactic foam under compression, *Compos. Part A Appl. Sci. Manuf.*, 35, 9, 1009–1015, 2004, doi: 10.1016/j.compositesa.2004.03.013.

(16)   H. A. Ogbunugafor *et al.*, Physico-chemical and antioxidant properties of Moringa oleifera seed oil, *Pakistan J. Nutr.*, 10, 5, 409–414, 2011, doi: 10.3923/pjn.2011.409.414.

(17)   A. H, *Handbook of Plastic Foams: Types, Properties, Manufacture and Applications*. Elsevier, 1995.

(18)   O. A. Afolabi, K. Kanny, and T. P. Mohan, Processing of hollow glass microspheres (HGM) filled epoxy syntactic foam composites with improved structural characteristics,

Sci. Eng. Compos. Mater., 28, 1, 116–127, 2021, doi: 10.1515/secm-2021-0011.

(19) M. Doddamani, Wear behavior of glass microballoon based closed cell foam, *Mater. Res. Express*, 6, 11, 2019, doi: 10.1088/2053-1591/ab446a.

(20) K. Shahapurkar, M. Doddamani, and G. C. M. Kumar, Tensile behavior of cenosphere/epoxy syntactic foams Mechanical characterization of Al-2024 reinforced with fly ash and E-glass by stir casting method AIP Conference Capacitive sensor for engine oil deterioration measurement AIP Conference Electrochemical studies of aluminium 7075 reinforced with Al 2 O 3 /SiCp hybrid composites in acid chloride medium AIP Conference, pp. 20109, 1943, doi: 10.1063/1.5029676.

(21) Sci-Hub | Mechanical properties of silica fume reinforced epoxy glass microballoons syntactic foams. Materials Today: Proceedings, 46, 672–676 | 10.1016/j.matpr.2020.11.745. https://sci-hub.se/https://doi.org/10.1016/j.matpr.2020.11.745 (accessed Sep. 06, 2021).

(22) M. Dubey, A. Thakur, K. Vishwkarma, H. K. Mall, and M. Dhirendra Kumar, Development of epoxy-thermoplastic based syntactic foam for structural application, *Int. J. Res. Eng. Sci. ISSN*, 9, 39–43, Accessed: Sep. 06, 2021. [Online]. Available: www.ijres.org.

(23) Sci-Hub | Co-continuous hollow glass microspheres/epoxy resin syntactic foam prepared by vacuum resin transfer molding. Journal of Reinforced Plastics and Composites, 073168441985717 | 10.1177/0731684419857173. https://sci-hub.se/https://doi.org/10.1177/0731684419857173 (accessed Aug. 27, 2021).

(24) K. C. Yung, B. L. Zhu, T. M. Yue, and C. S. Xie, Preparation and properties of hollow glass microsphere-filled epoxy-matrix composites, *Compos. Sci. Technol.*, 69, 260–264, 2008, doi: 10.1016/j.compscitech.2008.10.014.

(25) T. Roques-Carmes, P. Marchal, A. Gigante, and S. Corbel, Stereolithography fabrication

and characterization of syntactic foams containing hollow glass microspheres, *Russ. Chem. Rev.*, 78, 4, 375, Apr. 2009, doi: 10.1070/RC2009V078N04ABEH003897.

(26) Sci-Hub | 3D printing of syntactic foam cored sandwich composite. Composites Part C: Open Access, 3, 100068 | 10.1016/j.jcomc.2020.100068. https://sci-hub.se/https://doi.org/10.1016/j.jcomc.2020.100068 (accessed Sep. 06, 2021).

(27) J. E. Spowart, N. Gupta, and D. Lehmhus, ADDITIVE MANUFACTURING OF COMPOSITES AND COMPLEX MATERIALS, *JOM*, 70, doi: 10.1007/s11837-018-2742-2.

(28) Q. Yu, Y. Zhao, A. Dong, and Y. Li, Accepted Manuscript Mechanical properties of EPS filled syntactic foams prepared by VARTM, *Compos. Part B*, 2017, doi: 10.1016/j.compositesb.2017.07.053.

(29) Y. Zhou, F. Pervin, L. Lewis, and S. Jeelani, Fabrication and characterization of carbon/epoxy composites mixed with multi-walled carbon nanotubes, in *Materials Science and Engineering: A*, 475, 1–2, 157–165.

(30) Y. Bin *et al.*, Effect of Ultrasonication on the Properties of Multi-walled Carbon Nanotubes/ Hollow Glass Microspheres/Epoxy Syntactic Foam, *J. Wuhan Univ. Technol. Sci. Ed. www.jwutms*, 2017, doi: 10.1007/s11595-017-1656-0.

(31) M. Koopman, K. K. Chawla, K. B. Carlisle, and G. M. Gladysz, Microstructural failure modes in three-phase glass syntactic foams, *J. Mater. Sci.*, 41, 13, 4009–4014, 2006, doi: 10.1007/s10853-006-7601-9.

(32) N. Gupta, R. Ye, and M. Porfiri, Comparison of tensile and compressive characteristics of vinyl ester/glass microballoon syntactic foams, *Compos. Part B Eng.*, 41, 3, 236–245, 2010, doi: 10.1016/j.compositesb.2009.07.004.

(33) N. Kumar, S. Mireja, V. Khandelwal, B. Arun, and G. Manik, Light-weight high-strength hollow glass microspheres and bamboo fiber based hybrid polypropylene composite:

A strength analysis and morphological study, *Compos. Part B Eng.*, 109, 277–285, 2017, doi: 10.1016/j.compositesb.2016.10.052.

(34) R. Shankar and S. Sankaran, Materials Science and Engineering A 412 (2005) 153-158 Gradient syntactic foams: Tensile strength, modulus and fractographic features, 2005, doi: 10.1016/j.msea.2005.08.017.

(35) N. Gupta and R. Nagorny, Tensile properties of glass microballoon-epoxy resin syntactic foams, *J. Appl. Polym. Sci.*, 102, 2, 1254–1261, 2006, doi: 10.1002/app.23548.

(36) A. Strauchs, A. Mashkin, and A. Schnettler, Effects of SiO 2 nanofiller on the properties of epoxy resin based syntactic foam, *IEEE Trans. Dielectr. Electr. Insul.*, 19, 2, 400–407, 2012, doi: 10.1109/TDEI.2012.6180231.

(37) M. Yu, P. Zhu, and Y. Ma, Effects of particle clustering on the tensile properties and failure mechanisms of hollow spheres filled syntactic foams: A numerical investigation by microstructure based modeling, *Mater. Des.*, 47, 80–89, 2013, doi: 10.1016/j.matdes.2012.12.004.

(38) M. Colloca, N. Gupta, and M. Porfiri, Tensile properties of carbon nanofiber reinforced multiscale syntactic foams, *Compos. Part B*, 44, 584–591, 2013, doi: 10.1016/j.compositesb.2012.02.030.

(39) K. R. Dando and D. R. Salem, The effect of nano-additive reinforcements on thermoplastic microballoon epoxy syntactic foam mechanical properties, doi: 10.1177/0021998317716267.

(40) R. Ciardiello, L. T. Drzal, and G. Belingardi, Effects of carbon black and graphene nano-platelet fillers on the mechanical properties of syntactic foam, 2017, doi: 10.1016/j.compstruct.2017.07.057.

(41) H. S. Ashrith, M. Doddamani, and V. Gaitonde, Accepted Manuscript Effect of wall thickness and cutting parameters on drilling of glass microballoon/ epoxy syntactic foam

composites, 2018, doi: 10.1016/j.compstruct.2018.12.022.

(42) N. Gupta, Kishore, E. Woldesenbet, and S. Sankaran, Studies on compressive failure features in syntactic foam material, *J. Mater. Sci.*, 36, 18, 4485–4491, 2001, doi: 10.1023/A:1017986820603.

(43) N. Gupta, S. Priya, R. Islam, and W. Ricci, Characterization of Mechanical and Electrical Properties of Epoxy-Glass Microballoon Syntactic Composites, *Ferroelectrics*, 345, 1, 1–12, 2006, doi: 10.1080/00150190601018002.

(44) B. Song, W. Chen, T. Yanagita, and D. J. Frew, Temperature effects on dynamic compressive behavior of an epoxy syntactic foam, 2004, doi: 10.1016/j.compstruct.2004.07.012.

(45) Sci-Hub | Study on the performance of syntactic foam reinforced by hybrid functionalized carbon nanotubes. Journal of Applied Polymer Science, 48586 | 10.1002/app.48586. https://sci-hub.se/https://doi.org/10.1002/app.48586 (accessed Aug. 21, 2021).

(46) C. Swetha and R. Kumar, Quasi-static uni-axial compression behaviour of hollow glass microspheres/epoxy based syntactic foams, *Mater. Des.*, 32, 8–9, 4152–4163, 2011, doi: 10.1016/j.matdes.2011.04.058.

(47) X. Wu *et al.*, Preparation and Characterization of Three Phase Epoxy Syntactic Foam Filled With Carbon Fiber Reinforced Hollow Epoxy Macrospheres and Hollow Glass Microspheres, doi: 10.1002/pc.23205.

(48) Sci-Hub | Study on the performance of syntactic foam reinforced by hybrid functionalized carbon nanotubes. Journal of Applied Polymer Science, 48586 | 10.1002/app.48586. https://sci-hub.se/https://doi.org/10.1002/app.48586 (accessed Sep. 05, 2021).

(49) A. Yasmin, J. J. Luo, J. L. Abot, and I. M. Daniel, Mechanical and thermal behavior of

clay/epoxy nanocomposites, *Compos. Sci. Technol.*, 66, 14, 2415–2422, Nov. 2006, doi: 10.1016/J.COMPSCITECH.2006.03.011.

(50) T. M. Robert, S. Nair, D. Mathew, and C. P. Reghunadhan Nair, Room temperature processable heat-resistant epoxy-oxazolidone-based syntactic foams, *Polym. Adv. Technol.*, 29, 1, 121–129, 2018, doi: 10.1002/pat.4094.

(51) A. K. Ghamsari, S. Wicker, and E. Woldesenbet, Bucky syntactic foam; Multi-functional composite utilizing carbon nanotubes-ionic liquid hybrid, *Compos. Part B Eng.*, 67, 1–8, 2014, doi: 10.1016/j.compositesb.2014.06.030.

(52) C. Kanchanomai, N. Noraphaiphipaksa, and Y. Mutoh, Wear characteristic of epoxy resin filled with crushed-silica particles, *Compos. Part B Eng.*, 42, 6, 1446–1452, Sep. 2011, doi: 10.1016/J.COMPOSITESB.2011.04.046.

(53) J. Lee and A. F. Yee, Fracture of glass bead/epoxy composites: on micro-mechanical deformations, *Polymer (Guildf).*, 41, 23, 8363–8373, Nov. 2000, doi: 10.1016/S0032-3861(00)00187-7.

(54) Sci-Hub | Fracture toughness of rigid polymeric foams: A review. Fatigue & Fracture of Engineering Materials & Structures | 10.1111/ffe.13327, Accessed: Aug. 23, 2021. [Online]. Available: https://sci-hub.se/https://doi.org/10.1111/ffe.13327.

(55) H. S. Kim and M. A. Khamis, Fracture and impact behaviours of hollow micro-sphere/epoxy resin composites, Accessed: Aug. 23, 2021. [Online]. Available: www.elsevier.com/locate/compositesa.

(56) E. M. Wouterson, F. Y. C. Boey, X. Hu, and S.-C. Wong, Specific properties and fracture toughness of syntactic foam: Effect of foam microstructures, 2005, doi: 10.1016/j.compscitech.2005.03.012.

(57) Sci-Hub | Effect of composition on the fracture toughness and flexural strength of syntactic foams. Polymer Composites, 25(2), 229–236 | 10.1002/pc.20018. https://sci-

hub.se/https://doi.org/10.1002/pc.20018 (accessed Sep. 04, 2021).

(58) M. H. Woldemariam, G. Belingardi, E. G. Koricho, and D. T. Reda, Effects of nanomaterials and particles on mechanical properties and fracture toughness of composite materials: a short review, 2019, doi: 10.3934/matersci.2019.6.1191.

(59) A. Asif, V. L. Rao, and K. N. Ninan, Nanoclay reinforced thermoplastic toughened epoxy hybrid syntactic foam: Surface morphology, mechanical and thermo mechanical properties, *Mater. Sci. Eng. A*, 527, 6184–6192, 2010, doi: 10.1016/j.msea.2010.06.058.

(60) G. Gao, Y. Hu, H. Jia, P. Liu, P. Du, and D. Xu, Acoustic and dielectric properties of epoxy resin/hollow glass microsphere composite acoustic materials, *J. Phys. Chem. Solids*, 135, 109105, 2019, doi: 10.1016/j.jpcs.2019.109105.

(61) J. P. Ansermet and E. Baeriswyl, Dielectric study of hollow microsphere composites, *J. Mater. Sci.*, 29, 2841–2846, 1994.

(62) A. Strauchs, Impact of a silane-coating of hollow glass microspheres on the electrical properties of syntactic foam.

(63) D. Winkel, R. Puffer, and A. Schnettler, Investigation on the dielectric material parameters and the electric conductivity of syntactic foam at the liquid nitrogen temperature range, *IEEE Trans. Appl. Supercond.*, 25, 3, 7700605, 2015, doi: 10.1109/TASC.2014.2376190.

(64) B. Zhu, J. Ma, J. Wang, J. Wu, and D. Peng, Journal of reinforced plastics and composites, *J. Reinf. Plast. Compos.*, doi: 10.1177/0731684412452918.

(65) D. Mishra and A. Satapathy, An investigation on the dielectric properties of epoxy filled with glass micro-spheres and boron nitride.

(66) H. Ahmad *et al.*, Stealth technology: Methods and composite materials—A review, *Polym. Compos.*, 40, 12, 4457–4472, 2019, doi: 10.1002/pc.25311.

(67) G. A. Rao and S. P. Mahulikar, Integrated review of stealth technology and its role in

airpower, *Aeronaut. J.*, 106, 1066, 629–642, 2002.

(68) J. M. Headrick and J. F. Thomason, Applications of high-frequency radar, 33, 4, doi: 10.1029/98RS01013.

(69) S. Mishra, A. Dubey, H. B. Bhaskey, A. Soni, A. Dixit, and N. Eswara Prasad, Functional polymer matrix composites for structural and stealth applications, *Trans. Indian Inst. Met.*, 72, 6, 1659–1662, 2019, doi: 10.1007/s12666-019-01634-y.

(70) Sci-Hub | Polymer matrix composites as broadband radar absorbing structures for stealth aircrafts. *J. Appl. Polym. Sci.*, 47241 | 10.1002/app.47241. https://sci-hub.se/https://doi.org/10.1002/app.47241 (accessed Sep. 05, 2021).

(71) X. C. Tong, Advanced materials and design for electromagnetic interference shielding, *Adv. Mater. Des. Electromagn. Interf. Shield.*, Apr. 2016, doi: 10.1201/9781420073591.

(72) Z. Ali, B. Muneer, B. S. Chowdhry, S. Jehangir, B. Shankar Chowdhry, and G. Hyder, Article in International Journal of Wireless and Microwave Technologies · April 2020 I. J. *Wire. Micro. Technol.*, 2, 22–29, 2020, doi: 10.5815/ijwmt.2020.02.03.

(73) Sci-Hub | Broadband and Tunable RCS reduction using high-order reflections and salisbury-type absorption mechanisms. *Sci. Rep.*, 9(1) | 10.1038/s41598-019-45501-8. https://sci-hub.se/https://doi.org/10.1038/s41598-019-45501-8 (accessed Sep. 05, 2021).

(74) A. F. Kurniawan, M. Syaiful Anwar, K. Nadiyyah, M. Mashuri, T. Triwikantoro, and D. Darminto, Thickness optimization of a double-layered microwave absorber combining magnetic and dielectric particles, *Mater. Res. Express*, 8, 65001, 2021, doi: 10.1088/2053-1591/ac04ea.

(75) Sci-Hub | The two-sheet capacitive Jaumann absorber. IEEE Transactions on Antennas and Propagation, 43(11), 1339–1343 | 10.1109/8.475112. https://sci-hub.se/10.1109/8.475112 (accessed Sep. 05, 2021).

(76) Y. W. Nam, J. H. Choi, W. J. Lee, and C. G. Kim, Fabrication of a thin and lightweight

microwave absorber containing Ni-coated glass fibers by electroless plating, *Compos. Sci. Technol.*, 145, 165–172, 2017, doi: 10.1016/j.compscitech.2017.04.009.

(77)   J. H. Oh, K. S. Oh, C. G. Kim, and C. S. Hong, Design of radar absorbing structures using glass/epoxy composite containing carbon black in X-band frequency ranges, *Compos. Part B Eng.*, 35, 1, 49–56, 2004, doi: 10.1016/j.compositesb.2003.08.011.

(78)   C. G. Jayalakshmi, A. Anand, B. Kandasubramanian, and M. Joshi, High temperature composite materials for electromagnetic applications through a cost effective manufacturing process; Resin film infusion, *Mater. Today Proc.*, 33, 2217–2222, 2019, doi: 10.1016/J.MATPR.2020.03.804.

(79)   R. Kumar, D. Singh, T. C. Shami, H. B. Baskey, and N. Eswara Prasad, Design, fabrication and evaluation of low density, broadband microwave absorbing composite for X & Ku band, *2nd Int. Conf. Commun. Control Intell. Syst. CCIS 2016*, 198–202, 2017, doi: 10.1109/CCIntelS.2016.7878230.

(80)   S. Dasgupta, Polymer Matrix Composites for Electromagnetic Applications in Aircraft Structures, *J. Indian Inst. Sci.*, 95, 3, 275–296, Sep. 2015, Accessed: Sep. 05, 2021. [Online]. Available: http://journal.library.iisc.ernet.in/index.php/iisc/article/view/4573.

(81)   I. Hamerton and J. N. Hay, High Performance Polymers Recent Technological Developments in Cyanate Ester Resins, doi: 10.1088/0954-0083/10/2/001.

(82)   Sci-Hub | Radar Transparent, Impact Resistant and High Temperature capable Radome Composites using Polyetherimide (PEI) Toughened Cyanate Ester Resins for High Speed Aircrafts through Resin Film Infusion. Industrial & Engineering Chemistry Research | 10.1021/acs.iecr.9b06439.   https://sci-hub.se/https://doi.org/10.1021/acs.iecr.9b06439 (accessed Sep. 05, 2021).

(83)   K.-Y. Park, J.-H. Han, J.-B. Kim, and S.-K. Lee, Two-layered electromagnetic wave-absorbing E-glass/epoxy plain weave composites containing carbon nanofibers and NiFe

particles, doi: 10.1177/0021998311410467.

(84) J.-B. Kim, Advanced composite materials broadband radar absorbing structures of carbon nanocomposites broadband radar absorbing structures of carbon nanocomposites, 2012, doi: 10.1080/09243046.2012.736350.

(85) A. Ashraf *et al.*, Design of Carbon/Glass/Epoxy-Based Radar Absorbing Composites: Microwaves Attenuation Properties, doi: 10.1002/pen.23801.

(86) P. Mehdizadeh and H. Jahangiri, Effect of carbon black content on the microwave absorbing properties of CB/epoxy composites, *J. Nanostruct*, 6, 2, 140–148, 2016, doi: 10.7508/jns.2016.02.006.

(87) Sci-Hub | Design of Radar Absorbing Structures Utilizing Carbon-Based Polymer Composites. Polymers and Polymer Composites, 26(1), 105–110 | 10.1177/096739111802600113. https://sci-hub.se/https://doi.org/10.1177/096739111802600113 (accessed Sep. 05, 2021).

(88) S.-E. Lee, J.-H. Kang, and C.-G. Kim, Fabrication and design of multi-layered radar absorbing structures of MWNT-filled glass/epoxy plain-weave composites, 2006, doi: 10.1016/j.compstruct.2005.11.036.

(89) D. K. Ghodgaonkar, V. V Varadan, and V. K. Varadan, A Free-Space Method for Measurement of Dielectric Constants and Loss Tangents at Microwave Frequencies, 37, 3, 1989.

(90) P. C. Kim and D. Gil Lee, Composite sandwich constructions for absorbing the electromagnetic waves, 2008, doi: 10.1016/j.compstruct.2008.05.015.

(91) Sci-Hub | Design of Radar Absorbing Structures Utilizing Carbon-Based Polymer Composites. Polymers and Polymer Composites, 26(1), 105–110 | 10.1177/096739111802600113. https://sci-hub.se/https://doi.org/10.1177/096739111802600113 (accessed Sep. 01, 2021).

(92) C. E. Browning, The Mechanisms of Elevated Temperature Property Losses in High Performance Structural Epoxy Resin Matrix Materials After Exposures to High Humidity Environments*.

(93) K. J. Vinoy and R. M. Jha, Trends in radar absorbing materials technology, 20, 815–850, 1995.

(94) J. A. King, D. R. Klimek, I. Miskioglu, and G. M. Odegard, Mechanical Properties of Graphene Nanoplatelet/Epoxy Composites, *J. Appl. Polym. Sci*, 128, 4217–4223, 2012, doi: 10.1002/app.38645.

(95) A. Inamdar, J. Cherukattu, A. Anand, and B. Kandasubramanian, Thermoplastic toughened high temperature Cyanate esters and its application in advanced composites, 2018, doi: 10.1021/acs.iecr.7b05202.

(96) S. Tyagi, Ramesh, C. Agarwala, and V. Agarwala, Reaction kinetic, magnetic and microwave absorption studies of SrFe 11.2 Ni 0.8 O 19 hexaferrite nanoparticles, doi: 10.1007/s10854-010-0265-x.

(97) W.-H. Choi and C.-G. Kim, Broadband microwave-absorbing honeycomb structure with novel design concept, *Compos. Part B*, 83, 14–20, 2015, doi: 10.1016/j.compositesb.2015.08.027.

(98) Q. Zheng, H. Fan, J. Liu, Y. Ma, and L. Yang, Hierarchical lattice composites for electromagnetic and mechanical energy absorptions, *Compos. Part B Eng.*, 53, 152–158, 2013, doi: 10.1016/j.compositesb.2013.04.057.

(99) V. K. Chakradhary, S. Juneja, and M. Jaleel Akhtar, Correlation between EMI shielding and reflection loss mechanism for carbon nanofiber/epoxy nanocomposite, *Mater. Today Commun.*, 25, 101386, 2020, doi: 10.1016/j.mtcomm.2020.101386.

(100) M. Wu *et al.*, Constructing different categories of heterostructured magnetic nanoparticles@carbon nanotubes-reduced graphene oxide, and their tunable excellent

microwave absorption capabilities, *J. Alloys Compd.*, 785, 1126–1136, May 2019, doi: 10.1016/J.JALLCOM.2019.01.272.